# SIMPLE ZERO DIMENSIONAL QUASI-PREDICTIVE THERMODYNAMIC SIMULATION FOR PREDICTION OF NOx FOR DIESEL COMBUSTION

A Thesis

by

RYAN ALEXANDER BANDURA

Submitted to the Office of Graduate and Professional Studies of
Texas A&M University
in partial fulfillment of the requirements for the degree of

MASTER OF SCIENCE

| | |
|---|---|
| Chair of Committee, | Timothy J. Jacobs |
| Committee Members, | Jerald Caton |
| | Adonios Karpetis |
| Head of Department, | Andreas Polycarpou |

May 2017

Major Subject: Mechanical Engineering

# ABSTRACT

Computational fluid dynamics (CFD) is now a ubiquitous computational tool for engine design and analysis. It is often necessary to provide well-known initial cycle conditions to commence the CFD computations. Such initial conditions can be provided by experimental data. To create an opportunity to computationally study engine conditions where experimental data are not available, a zero-dimensional quasi-predictive thermodynamic simulation is developed that uses a well-established spray model to predict rate of heat release and calculated burned gas composition and temperature to predict nitric oxide (NO) concentration. This thesis details the thermodynamic simulation for diesel engine operating conditions. The goal is to produce an algorithm that is capable of predicting NO emissions as well as performance characteristics such as mean effective pressure (MEP). The simulation uses general conservation of mass and energy approaches to model intake, compression, and exhaust. Rate of heat release prediction is based on an existing spray model to predict how fuel concentrations within the spray jet change with penetration. Rate of heat release provides predicted cylinder pressure, which is then validated against experimental pressure data under known operating conditions. An equilibrium mechanism is used to determine burned gas composition which, along with burned gas temperature, can be used for prediction of NO in the cylinder. NO is predicted using the extended Zeldovich mechanism. This mechanism is highly sensitive to temperature, and it is therefore important to accurately predict cylinder gas temperature to obtain correct NO values.

The simulation focuses on single fuel injection events, but some multiple injection events are investigated, and improvements to the model to better handle these cases are suggested.

# ACKNOWLEDGEMENTS

My committee chair, Dr. Timothy Jacobs must first be acknowledged. He has helped me through every step of the process of obtaining my degree. I do not believe that had I had any other advisor I would have been nearly as successful. I would also like to thank my other committee members, Dr. Caton and Dr. Karpetis, for their support in the creation of this research.

I have had opportunities here at Texas A&M University for which I am incredibly grateful. I have been given every opportunity to succeed and given access to invaluable resources. I would like to thank all of the students and staff members with whom I have had the pleasure to work the last two years. I would also like to thank everyone for their patience. My situation was unusual and difficult, so it has delayed this final product. However, no one has stopped believing in me, and for that I am grateful.

Finally, I would like to thank my family for their continued support throughout this process. I travelled halfway across the country to this incredible university, and their support was unwavering.

# CONTRIBUTORS AND FUNDING SOURCES

This work was supported by a thesis committee consisting of Professor Jacobs, Professor Polycarpou of the Department of Mechanical Engineering, and Professors Karpetis of the Aerospace Engineering Department.

Graduate study and the data analyzed in this work was provided by a sponsoring agency that wishes to remain anonymous.

# NOMENCLATURE

## Variables

| | |
|---|---|
| a | EGR-based temperature reduction exponent |
| AF | Air-fuel ratio |
| AFMEP | Auxiliary Friction Mean Effective Pressure (kPa) |
| BMEP | Brake Mean Effective Pressure (kPa) |
| C | Concentration ($g/cm^3$) |
| CFMEP | Crankshaft Friction Mean Effective Pressure (kPa) |
| d | Injector nozzle diameter (m) |
| dm | Change in mass (kg) |
| dm/ds | Change in mass per penetration length (kg/m) |
| dm/dt | Change in mass per unit time (kg/s) |
| dR/ds | Change in jet radius per penetration length |
| ds/dt | Change in penetration per unit time (m/s) |
| $\delta Q/dt$ | Rate of heat release (J/s) |
| $\varepsilon$ | Dimensionless radius, r/R |
| $\gamma$ | Ratio of specific heats |
| IMEP | Indicated Mean Effective Pressure (kPa) |
| KLA | Model specific parameter |
| l | Injector nozzle length (m) |
| LHV | Lower heating value (kJ/kg) |

| | |
|---|---|
| $\lambda$ | Air ratio |
| M | Molar mass (kg/kmol) |
| $\dot{m}$ | Mass flow rate (kg/s) |
| $\mu$ | Nozzle discharge coefficient |
| n | Number of moles |
| p | Pressure (kPa) |
| PMEP | Pumping Mean Effective Pressure (kPa) |
| Q | Integrated heat release (J) |
| r | Radius at desired concentration (m) |
| R | Total jet radius (m) |
| $\bar{R}$ | Universal gas constant (kJ/K-mol) |
| $\rho$ | Density ($kg/m^3$) |
| RFMEP | Reciprocating Friction Mean Effective Pressure (kPa) |
| $RFMEP_{gas}$ | Reciprocating Friction Mean Effective Pressure with Gas Pressure Loading (kPa) |
| s | Jet penetration (m) |
| t | Time (s) |
| T | Temperature (K) |
| TFMEP | Total Friction Mean Effective Pressure (kPa) |
| $\tau$ | Engine Torque (N-m) |
| u | Jet velocity (m/s) |
| V | Cylinder volume ($m^3$) |
| Vd | Displaced volume ($m^3$) |

| | |
|---|---|
| VFMEP | Valvetrain Friction Mean Effective Pressure (kPa) |

## Exponents/Subscripts

| | |
|---|---|
| 0 | Initial |
| a | Air/gas |
| avg | Average |
| bz | Burned zone |
| c | Centerline |
| e | Equilibrium |
| f | Fuel |
| F | Jet front |
| fbl | Between flammability limits |
| fprep | Prepared fuel |
| g | Global variable |
| g0 | Global variable at the start of injection |
| inj end | Injection end |
| l | Lower flammability limit |
| n | Nozzle parameters |
| n | Polytropic exponent |
| s | Stoichiometric |
| st | Stoichiometric |

| | |
|---|---|
| u | Upper flammability limit |
| uz | Unburned zone |

# TABLE OF CONTENTS

Page

# LIST OF FIGURES

Page

# LIST OF TABLES

Page

# 1. INTRODUCTION

## 1.1 Motivation

Providing accurate emissions profiles is key in ensuring that a given engine will meet government regulatory standards. CFD is an essential element in the engineer's arsenal to rigorously determine if this will be the case. In order to begin CFD simulations, however, initial cylinder conditions often must be known. These can be obtained with experimental data. In the absence of experimental data, however, a zero-dimensional quasi-predictive thermodynamic simulation can provide reasonably accurate initial conditions. This thesis describes the development of such a simulation. A well-established spray model is used to predict rate of heat release as well as burned gas composition and temperature. With an accurate temperature prediction, it is possible to predict nitric oxide concentration. This is the ultimate goal, along with predicting some other performance parameters such as mean effective pressure; in other words, operating conditions can be specific by BMEP, BSFC, and NO emissions targets to dictate the engine operating conditions to be studied with CFD.

This simulation focuses on single injection events. Multiple injection events, however, are also examined albeit with a lower accuracy. For this study, it is assumed that the rate of injection profile is rectangular if no rate of injection profile is known. Based on intake manifold pressure at the start of compression (i.e., another input), the

temperature and pressure at the start of injection can be determined using a simple polytropic model. A series of equations is developed with the intent of modeling the rate of heat release (ROHR) of the engine. Once ROHR has been accurately modeled, it is possible to predict the temperature and pressure in the cylinder. Temperature and equivalence ratio (determined from a well-defined spray model) are used to determine the composition of the cylinder using equilibrium mechanisms. Finally, nitric oxide can be calculated for the combustion process.

### 1.2 Background

There are many zero-dimensional quasi-predictive simulations currently in existence. Many of these models are not completely predictive and require some operating parameter to be experimentally determined. Two approaches are utilized in this work.

The first approach is presented by Eilts and Stoeber-Schmidt [1]. This work focused on medium speed diesel engines and was determined to be applicable to medium and upper load ranges. These engines were mostly larger displacement engines; most cases are analyzed for 200 mm and 320 mm bores. However, two additional cases calculate ROHR for an 81 mm bore engine. EGR was 0, 20, or 25%. The maximum loads were not given for each engine, but the authors explicitly stated that the cases were medium to high load. Plots were provided depicting the cylinder pressure and ROHR, and most cases matched well. As will be described later, the premixed spike for ROHR is not well captured by the algorithm for any cases. Using a model for both steady and

unsteady jets, the ROHR could be predicted with a reasonable degree of accuracy. One of the more unique aspects of [1] is that it avoids the necessity of an ignition delay approximation. Combustion is determined to occur when the concentration of the air-fuel mixture approaches a certain value. This lack of ignition delay correlation enhances simplicity and reduces the number of constants required for tuning a specific engine. This is highly desirable as this simulation is intended to be applied to a wide range of operating conditions and engine geometries. Some alterations to [1] were necessary for application to the cases in this study. These changes are detailed in the model description section, but they must first be justified. The methods of [1] focus primarily on larger bore diesel engines at medium to high loads and generally at lower speeds. Most cases analyzed in [1] were at 1000 RPM or lower. The current work studies cases with engine speeds in the range of 1300 to 2400 rpm. While most of the parameters are similar to those found in [1], many are different, thus necessitating some differences between that model and the one developed herein. As noted, the operating speed is different and there are some low load cases. Additionally, the engine geometries are smaller than those used to develop [1], so some departure is naturally expected.

The second approach is presented by Wilhelmsson et al. [2]. This uses a physical two-zone model to predict engine-out NO emissions. Burned and unburned zones are used to determine temperature, and the extended Zeldovich mechanism is used for NO prediction. The method described by Wilhelmsson et al. [2] was selected in a comparison against a method described by Querel et al. [3]. The method of [2] is very similar to that used in [3] in terms of burned zone volume and moles in each zone. The

method of calculating the burned zone temperature in [2], however, is much simpler without any penalty in accuracy; so this was chosen as the preferred method. Querel et al. [3] uses experimental pressure as does [2], but requires iteration to determine adiabatic temperature. Many works make this assumption, but it is avoided here to improve computational run times. The method of [2] avoids iteration, thus enabling faster run times. Much of [2] is rooted simply in the ideal gas law, and this assumption is made elsewhere in the simulation. Since this inaccuracy is already accepted as reasonable as compared to the real gas behavior, applying it for the temperature predictions lends no further error. The temperature predictions are smooth and do not deviate from the expected temperature ranges. The difficulty occurs with estimating the burned zone temperature because this is very challenging to measure experimentally. The correlations provided by [2] appear to produce results that are reasonable, and the predicted NO is close to the experimental values. Contrary to the ROHR calculations, the methods of [2] are largely unchanged in this model. Direct comparisons between the predicted temperatures in [2] and those predicted here are not appropriate, but the temperature ranges match well. This helps build confidence that the algorithm was correctly implemented.

The most widely accepted spray model is Hiroyasu et al [4]. This model is not used here in favor of that used in [1]. Spray penetration characteristics between the two models were compared, however, to ensure reasonable values from that of [1]; and the predictions were similar. The comparison between [1] and [4] was an important step. It helped to lend credibility to the methods provided in [1] as well as confirmed that the

correlations were accurately coded. In all cases, the spray penetration impinged the cylinder wall. Impingement was said to occur when the spray reached a distance of the bowl radius from the injector nozzle.

NO prediction is often done using the three step Zeldovich model. Heywood has distilled this to a single step algorithm, and this is widely accepted [5]. This work will retain the original three step extended Zeldovich model, an evolution of which is in [2]. This three step version is very convenient as it utilizes equilibrium concentrations to obtain the non-equilibrium NO. In most cases, the equilibrium concentrations of the supporting species (such as monatomic oxygen, nitrogen, and equilibrium NO) are provided by correlations that are readily available. Additionally, with the approaches listed in [1] it is possible to determine the equivalence ratio of the combusting jet. With this information, simple equilibrium expressions can be applied to obtain concentrations of all other species such as carbon monoxide, carbon dioxide, and water.

Another approach for NO prediction is seen in [6] and [7]. A large amount of experimental data is obtained and a statistical model is generated to predict NO concentration. Such a model was not used due to the desire for a more comprehensive simulation that included ROHR and temperature predictions. Additionally, these models often require application of tuning parameters. These parameters can vary from engine to engine, so this approach is not desirable in this case. The simulation that was built for use here is intended for many operating conditions, so it would be impractical to utilize tuning constants that must be individually picked for every operating condition or even

every engine. Additionally, there is another simple reason the statistical method was not utilized here: the amount of data was not sufficient to produce correlations with confidence.

NO predictions are very sensitive to temperature, so the temperature model used is crucial for an accurate prediction. Many groups such as [8] and [9] often use adiabatic flame temperature for the NO solution. However, it is difficult to determine if the adiabatic flame temperature is an accurate representation of the cylinder temperature in the burned gas region. Instead, a two zone model with "burned" and "unburned" temperatures is used. The burned zone temperature is not necessarily the adiabatic flame temperature, but rather an average representation of the gas temperatures the NO producing regions are likely to encounter. The predictions are compared qualitatively to those in [2], and they were found to be reasonable.

Another layer of complexity can be introduced with a transient model, as described in Finesso and Spessa [10]. Finesso and Spessa [10] uses a three zone model to analyze an engine under non-steady state conditions. While this approach could be implemented here, it is deemed to be too time consuming and not worth the tradeoff in computational expense for the increased accuracy. Further, the CFD simulations this simple model is meant to support makes calculations under steady conditions. Thus, the methods used in this work assume steady state operating conditions.

The output goal of this simulation is to generate NO predictions within ten percent of the experimental NO values. This ten percent goal is not necessarily

ambitious, but very slight changes in temperature can lead to NO predictions that are orders of magnitude different. It is believed the burned zone temperature prediction given by [2] contains sufficient accuracy to predict NO within ten percent. Additionally, the experimental data used for the tuning and validation of this model was not transient but rather steady state.

As previously noted, this simulation focuses on the three-step Zeldovich mechanism. In realistic kinetics, there are other forms of NO production such as prompt and $N_2O$ mechanisms. These have been studied as in [11], but are being neglected in this analysis. They are present in reality, but the NO production is dominated by Zeldovich mechanism. The experimental apparatus is able to capture $NO_x$, but for this simulation this is assumed to be composed entirely of NO with no additional variants such as $NO_2$ or $NO_3$. This approach is generally accepted to be accurate and proves to be sufficient in this simulation.

In order for the engine cycle to be completely simulated, it is necessary to implement models for intake, compression, expansion and exhaust. The current work focuses heavily on expansion because it includes both the heat release and emissions formation processes as described above; the other three strokes can be determined without much difficulty. The pressures and temperatures are determined through the use of the conservation of energy equations for each step, and are taken from [5]. The mass entering and exiting the cylinder during the intake and exhaust processes can be determined from known valve profiles. With cylinder pressures known for the entire

cycle, and an appropriate friction model, performance parameters such as indicated mean effective pressure (IMEP) and brake mean effective pressure (BMEP) can be calculated. These mean effective pressure values are important for determination of how an engine is performing and a critical part of the simulation. To obtain BMEP from IMEP, an engine friction model must be implemented. The model chosen here is found in [12] and is very comprehensive. It accounts for friction losses from all potential components of the engine. Rubbing friction for the crankshaft, valvetrain, and reciprocating components is quantified as well as pumping and auxiliary losses.

The models used in this simulation are far from the only models available. While the rate of heat release (ROHR) was modeled using [1], there are many other plausible means of ROHR determination. A common method is called the Double Wiebe function, represented in [13]. It uses a series of tunable constants to model ROHR accurately, and can match experimental data very well. The constants account for the length of the premixed spike, the diffusion flame duration, ignition delay, injection duration, engine speed, air-fuel ratio, and fuel injected. This can be done with iterative calculations, but constants must be tuned carefully for *every* operating condition. As previously detailed, this simulation is intended for use on a wide range of engine geometries and operating cases, so the Double Wiebe function is not very useful here. It would be impractical to spend time tuning the function to accurately match the experimental ROHR for every case; additionally, ROHR is not the targeted performance parameter for this simulation so extreme accuracy is not necessary. Therefore, the methods in [1] have been deemed acceptable for this particular application.

In addition to the widely-used Double Wiebe function, there are also highly-correlated approaches that are similar in background theory. One such approach is described by Walke, et al. [14]. Once again, this approach is not nearly as rigorous or as predictive as [1], but it can be used as a means of comparison. There are three constants that must be tuned for various engine geometries, and [14] is more or less a fitment approach for approximating ROHR. The details of the three constants are scarce in this approach, but they are part of a weight factor used for correlating the premixed and diffusive burning rate of the fuel. As a result, it lacks predictability that can be applied to a wide variety of engines, as is the goal for this simulation. With just three constants used for tuning, however, it is not difficult to implement this approach to obtain a model that must be tailored for each case. Additionally, in the absence of intake and exhaust valve profiles [14] suggests a polytropic approach for compression pressure modeling. This particular approach is assumed to be adiabatic, an assumption not made in the current simulation. The current study made an attempt to match the method used in [14] to the current engine cases, but found that no amount of tuning could produce results that were accurate. The simplicity of this model was certainly attractive, but the complete inability to produce a simulation even remotely close to real-world results disqualified it from use.

Complete understanding of the diesel combustion cycle necessitates analysis of the typical ROHR curve. This is important for validation of the diesel spray model and understanding how it captures the process. The phases of combustion are nicely summarized in [15]. The initial phase after the start of injection is the ignition delay

phase. During the ignition delay, almost no heat is released through combustion of the fuel. For combustion to occur, the fuel must meet and exceed the autoignition limits. In a diesel engine, these limits are eclipsed via the compression process. The end of this phase is often characterized for simulation purposes by a minimum threshold of heat release, usually set to be very small. Once this threshold has been reached, the fuel burning is said to be in the premixed combustion stage. This phase produces very fast burning rates, resulting in pressure rising very quickly. The premixed combustion occurs very quickly, and is essentially when the fuel between the upper and lower combustion limits burns almost spontaneously. The model used by [1] however, does not calculate an ignition delay. Instead, once a certain threshold of fuel concentration is reached, burning is allowed to commence. This sounds similar to how a diesel engine actually operates, but the main difference is that instead of a spontaneous combustion of large amounts of the injected fuel, the jet is reaching the combustion limits in small amounts. This is similar to what happens during the final phase of diesel combustion: the diffusion combustion. This final stage has burn rates that are mixing controlled and limited by the mixing rate, and a flame front can be detected. This is a much more linear burning of the fuel, and this is similar to the method described in [1]. As a result, the effects of the premixed combustion that typically takes place in a diesel engine are minimized and diffusion combustion is emphasized in the studied ROHR model. Medium and high load cases are often dominated by diffusion combustion, but in low load cases (and those with pilot injections) premixed combustion is much more important. As the results will show,

this model generally does not handle low load cases very well without application of external factors.

When designing a model intended specifically for NO prediction, it is important to take the effects of exhaust gas recirculation (EGR) into account. EGR is frequently used in modern diesel engines as a method for NO reduction. EGR is exactly as it sounds; exhaust gases are recycled through the engine. At medium and high load conditions, EGR is often used at higher rates. EGR rates up to 30% are not unusual, though most engines use less than this. In this simulation, all cases are using EGR at rates less than 15%. EGR reduces the NO emissions through the lowering of the peak combustion temperature [16]. The products of combustion from the previous cycle can actually absorb more heat than atmospheric air during the combustion process, and aid in keeping the temperature lower. These kinetics are very complex, and in this model are represented simply by a reduction of the temperature at the start of combustion. This leads to a reduced peak temperature relative to the same operation condition sans EGR.

### 1.3 Objective

The objective of this thesis is to develop a simple non-dimensional two-zone diesel engine simulation that can be predict the initial cylinder conditions for CFD analysis and exhaust NO emissions of various engine sizes operating at various loads. The simulation centers mostly on predicting medium to high load conditions; low load conditions are also addressed, but this model includes a spray penetration regime that is not well suited to low load combustion. This model requires few inputs and accounts for

exhaust gas recirculation (EGR) rates. The objective is also to create a model that requires minimal tuning, especially as compared to other approaches such as the Wiebe model.

Accomplishment of these objectives will lead to a simulation that can be used to estimate NO and could be used in concert with CFD to predict cylinder conditions with a high degree of accuracy. With this information, engineers can understand NO formation more completely and eventually reduce emissions.

# 2. DESCRIPTION OF THE MODEL

As described above, this simulation is a development on the approaches presented in [1] and [2]. It is assumed that the basic operating conditions of the engine, i.e., rate of injection profile, engine speed, and initial pressure, are known. Some aspects of the model are altered slightly in this simulation and as described in this thesis. In this model, a rectangular rate of injection profile is assumed if the rate of injection profile is not known. The rate is calculated with the use of the engine's BSFC at a given operating condition as well as torque and RPM. A block diagram for the code operating the simulation is provided in Figure 1 and a control system diagram is provided in Figure 2.

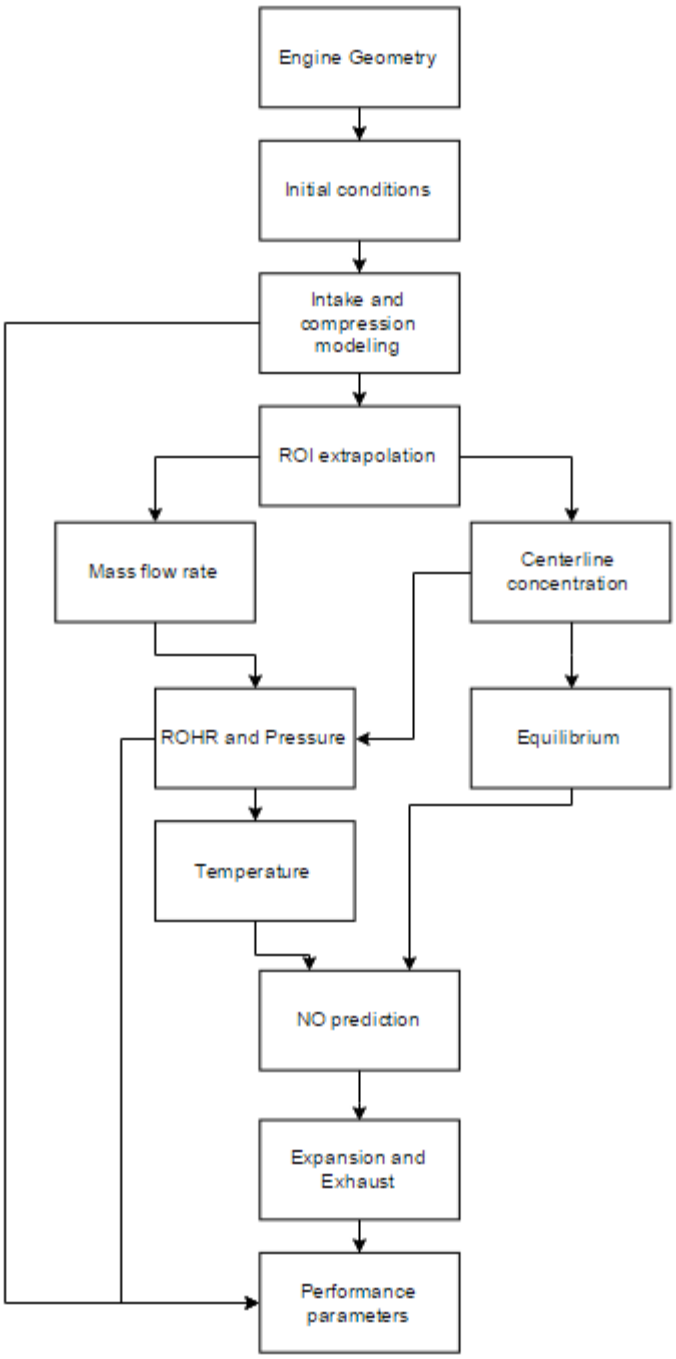


**Figure 1 - Block diagram for simulation.**

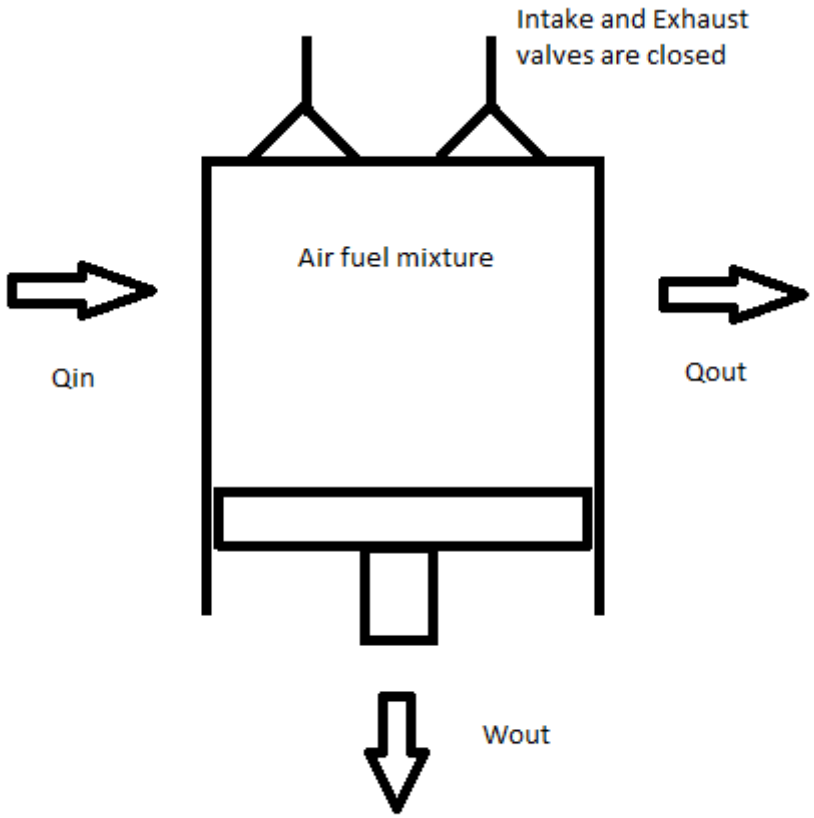


**Figure 2 – Control system representation.**

## 2.1 Engine Geometry

Engine geometry must be known in this simulation. This includes bore, stroke, compression ratio, connecting rod length, intake and exhaust valve diameter, wrist pin offset, injector nozzle diameter, bowl diameter, and number of orifices. The intake and

exhaust valve timing must also be known. The table below details the engine geometry for this particular study.

**Table 1 - Engine geometry.**

| | |
|---|---|
| **Displacement** | 4.5L |
| **Compression ratio** | 16.7 |
| **Bore** | 106.5 mm |
| **Stroke** | 127 mm |
| **Crank to wrist pin offset** | 0.3 mm |
| **Intake valve diameter** | 32.9 mm |
| **Exhaust valve diameter** | 32.27 mm |
| **Bowl diameter** | 8 mm |
| **Injector nozzle diameter** | 0.145 mm |
| **Injector nozzle length** | 0.2 mm |
| **Injector holes** | 6 |
| **H/C ratio** | 1.796 |

## 2.2 Initial Conditions

Initial conditions that must be given include the injection timing, intake manifold pressure and temperature, EGR rate, ROI profile, engine speed, injection pressure, and the desired crank angle resolution. Table 2 shows the conditions used in this work. Tables 3 and 4 show the additional cases used for model validation. The cases that do not use EGR are marked with an asterisk.

**Table 2 – Operating conditions and engine descriptors, multiple injection cases are marked "M" next to the injection timing.**

| Engine Mode | Speed (RPM) | EGR (%) | Injection timing | Intake Pressure (kPa) | BSFC | Injection pressure (kPa) |
|---|---|---|---|---|---|---|
| 1 | 1400 | 0 | -2.640M | 120.34 | 389.4 | 3668 |
| 2 | 1400 | 0 | 4.007M | 117.57 | 271.61 | 3827 |
| 3 | 1400 | 9.57 | -1.844 | 172.79 | 232.14 | 7789 |
| 4 | 1900 | 0 | -2.82M | 138.99 | 450.64 | 4156 |
| 5 | 1900 | 0 | -6.58 | 156.43 | 266.02 | 6314 |
| 6 | 1900 | 15.06 | -5.46 | 210.67 | 229.48 | 8940 |
| 7 | 2400 | 0 | -6.75M | 167.99 | 536.65 | 3889 |
| 8 | 2400 | 14.67 | -10.5 | 169.65 | 289.68 | 6492 |
| 9 | 2400 | 13.22 | -11.08 | 239.73 | 232.14 | 8645 |

**Table 3 - Operating conditions for 6.8L additional cases.**

| CASE | 1 | 2 | 3 | 4 | 5 | 6 | 7 | 8 | 9 | 10 | 11 | 12* | 13* | 14* | 15* | 16* | 17* | 18* | 19* | 20* | 21* | 22* | 23* |
|---|---|---|---|---|---|---|---|---|---|---|---|---|---|---|---|---|---|---|---|---|---|---|---|
| RPM | 2400 | 2000 | 1600 | 1400 | 1599 | 1400 | 2000 | 1600 | 1400 | 2399 | 2000 | 2400 | 1999 | 1600 | 1399 | 1600 | 1400 | 2000 | 2399 | 1600 | 1399 | 1999 | 2400 |
| Torque (N-m) | 891 | 1069 | 1245 | 1227 | 999 | 999 | 800 | 800 | 800 | 599 | 600 | 892 | 1069 | 1244 | 1226 | 999 | 1000 | 800 | 700 | 700 | 699 | 500 | 399 |

**Table 4 - Operating conditions for 9.0L additional cases.**

| Case | 1 | 2 | 3 | 4 | 5 | 6 | 7 | 8 | 9 | 10 | 11 | 12* | 13* | 14* | 15* | 16* | 17* | 18* | 19* | 20* | 21* | 22* | 23* | 24* |
|---|---|---|---|---|---|---|---|---|---|---|---|---|---|---|---|---|---|---|---|---|---|---|---|---|
| RPM | 1299 | 1599 | 1899 | 2199 | 2199 | 1899 | 1599 | 1299 | 2199 | 1899 | 1599 | 1299 | 1299 | 1599 | 1899 | 2199 | 1299 | 1599 | 1899 | 2199 | 2199 | 1899 | 1599 | 1299 |
| Torque (N-m) | 1679 | 1720 | 1560 | 1376 | 1163 | 1322 | 1454 | 1356 | 872 | 991 | 1090 | 1017 | 1679 | 1720 | 1560 | 1376 | 1186 | 1272 | 1157 | 1018 | 581 | 661 | 727 | 678 |

**Tables 3 and 4 – asterisk indicates no EGR.**

### 2.3 Intake and Compression

Intake modeling is very simple. The intake pressure is assumed to be that of the intake manifold. This is not the case in a real engine, but the approximation works in this scenario because intake pressure and temperature are not critical.

A simple polytropic model is used for the compression process. The initial pressure at inlet valve close is assumed to be known and equal to that of the intake manifold.

$$P(i) = P(i-1) \cdot \left(\frac{V(i-1)}{V(i}\right)^{n} \quad (1.1)$$

$$T(i) = T(i-1) \cdot \left(\frac{P(i}{P(i-1)}\right)^{\frac{n-1}{n}} \quad (1.2)$$

$$) \quad (1.3)$$

In equations (1.1-1.3), the “i” terms denote when the value should be taken. The “i-1” terms are at the previous iteration, while the “i” terms are at the current crank angle. The “n” value is the polytropic exponent. This approach was taken from [17] as a simple method of polytropic exponent determination. These methods proved accurate, so increased complexity was deemed unnecessary. The intake valve close timing is known, and this is used to determine when the start of compression occurs. This method works well, and as will be displayed the predicted compression curves match well with the experimental.

## 2.4 ROI Extrapolation and Fuel Mass Flow Rate

As previously noted, a rectangular rate of injection profile is assumed for the cases for which the profile is unknown. The engine's torque is used with BSFC to estimate the average rate of injection. Next, the effective rate of injection is found using as seen in (1.4).

$$\dot{m} = \dot{m}_{avg} \cdot shape \cdot factor \qquad (1.4)$$

In (1.4), the average rate of injection is that determined from BSFC. The "shape" parameter can be the imposed injection rate shape. In this work, a pseudo-rectangular injection profile is used based on the shape of an injection event for a similar engine. The similar engine is the 6.8L detailed further in the work, as the primary engine analyzed here is simply a four cylinder version of that six cylinder engine; geometrical details of the engine under study are provided in Table 2. The "shape" was first normalized in order to be used here, so multiplication of the average rate of injection is necessary along with a secondary "factor" parameter. This is a non-linear fifth order function of BSFC, intake manifold pressure, and engine speed as seen in (1.5). $P_{in}$ is in kPa and N is engine speed.

$$f_2 = \frac{BSFC}{P_{in} N} \qquad (1.5)$$

## 2.5 Spray Modeling / Centerline Concentration

The approach for modeling the injector spray is similar to that used in [1]. It is based on a quasi-steady state jet similar to that used by Hiroyasu [4] with some minor changes. It includes the introduction of a KLA factor for reacting jets that will be described in detail. The change in radius, dR, of the fuel spray per penetration length, ds, is a function of injector geometry only as seen in (1.6) and replicated from [1]. It is an empirical formula based on an equation cited in [1].

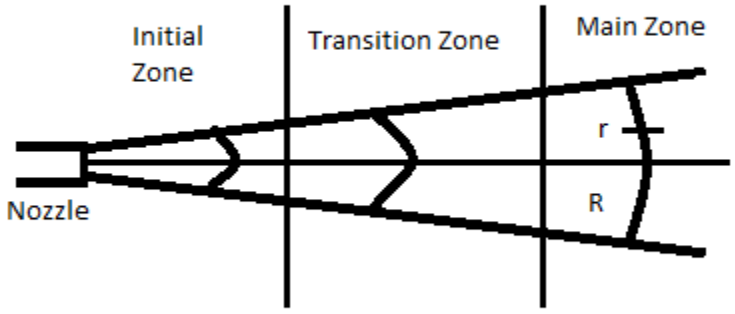


**Figure 3 - Change in radii as a function of jet penetration [1].**

Figure 3 shows how the radii vary as a function of jet penetration. It also shows the initial zone and transition zone. These zones were assumed to be so small as to be

negligible in [1], and that assumption is carried over here. The initial zone is that right after the nozzle, but the spray does not become well developed until the main zone. The initial and transition zones are difficult to model accurately, which is one of the reasons why they were not taken into account in [1] or here.

$$\frac{dR}{ds} = \frac{0.54}{3 + 0.07(\frac{l_N}{d_N})^{1.6}} \tag{1.6}$$

In equation (1.6), $l_N$ is the length of the injector nozzle hole, and $d_N$ is the diameter of the nozzle. The above formula is viable when $\frac{l_N}{d_N} < 5$. It should also be noted that for injectors with multiple openings, $d_N$ should be multiplied by the number of holes for all equations presented hereafter.

The authors of [1] introduced a parameter KLA that will be discussed now. This is a model tuning parameter, and in [1] it was assumed to be equal to 1 for non-reacting jets and not 1 otherwise. As a result, KLA accounts for jet reactivity. In this work KLA was determined to vary as a function of cylinder pressure and injection timing. This makes sense as the injection jet is strongly affected by pressure. The injection timing was also found to have an effect on KLA in that earlier injection timings necessitated significantly different KLA values than late timings. After the end of injection, it becomes a function of cylinder displacement. This is a deviation from [1], but it was found appropriate to account for the higher levels of premixed burn fraction and wider range of operating conditions. This was determined after analysis of predicted cylinder

pressure as compared to experimental cylinder pressure. This algorithm was applied to 48 operating cases, provided in Table 3 and Table 4, and works reasonably well for most of them as shown in the Results section.

$$t < t_{inj\ end} : KLA = [(2 - \frac{P}{10000}^{3}) + \left|\frac{inj\ time}{10}\right|] \cdot 0.325 \quad (1.7)$$

$$t \geq t_{inj\ end} : KLA = KLA \cdot 1.00025 + \ln(KLA \cdot 10)(Vd \cdot 100)^{3} \quad (1.8)$$

Equations (1.7) and (1.8) are introduced in the current study; KLA values in [1] were constant and generally less than one in [1]. However, it was not explicitly stated how the authors of [1] determined KLA. Therefore, it was necessary to devise some algorithm. The results are Equations (1.7) and (1.8). It was noted that to match experimental rate of heat release (ROHR) a change in KLA was necessitated between the injection duration and combustion after the end of injection. During injection, the pressure, $P$, and injection timing, $inj\ time$ (in degrees before top dead center), were used to determine KLA to accurately model the initial rate of change of the ROHR. After the injection was ended, the engine displacement, $Vd$, was used to recalculate KLA. This was used due to trends for varying engine displacements. The next concept to be introduced is that of the dimensionless radius, $\varepsilon = \frac{r}{R}$. R is the radius of the jet, and r is the radius of the jet at a desired concentration. Figure 3 is reproduced from [1] showing how the radius changes as a function of penetration.

$$C = C_c(1 - \varepsilon^{1.5}) \quad (1.9)$$

Equation (1.9) details how the concentration varies as a function of centerline fuel concentration, $C_c$, and ε. The centerline fuel concentration varies as a function of penetration and nozzle geometry as seen later in equation (1.12). Equation (1.9) can be used with a specified concentration to determine the radius at which that concentration occurs. This is the method employed here.

The nozzle diameter is assumed to be known and with a rate of injection profile imposed the initial velocity can be determined.

$$u_0 = \frac{4\dot{m}}{\pi \rho_f d_N^2} \tag{1.10}$$

In (1.10), $\dot{m}$ is the rate of injection, and $\rho_f$ is the density of the fuel. Equation (1.10), however, is only valid during injection. After the end of injection, the average value for the rate of injection is used in (1.10) as the jet's initial velocity.

Next, the penetration of the spray jet must be determined, as shown by Equation (1.11) [1].

$$s = \sqrt{\frac{1.14}{\frac{dR}{ds} KLA} u_0 d_N \sqrt{\frac{\mu \rho_f}{\rho_a}}}\, t \tag{1.11}$$

After impingement to the cylinder wall occurs, (1.11) is determined to have a constant value. Impingement is said to occur when penetration reaches the depth of the bowl radius. In this equation, $t$ is the time after the start of injection, $\rho_g$ is the density of the gas in the chamber, and $\mu$ is the nozzle discharge coefficient.

The next important parameter to consider is the centerline fuel concentration. This is a function of the change in radius per change in penetration, the nozzle geometry, the densities of the fuel and gas, and penetration length. The centerline concentration is important to determine ROHR because the burning rate is a function of how lean or rich the mixture is on the centerline of the fuel jet. This equation is slightly modified from that used in [1]. The constant was modified to be 0.75 because this more accurately modeled the engine geometries under investigation. The application of this provides a correction for the injector nozzle diameter. In [1], large diameters lead to a higher centerline concentration. However, in the present work, a modification is necessary to correctly model centerline concentration in smaller bore, higher speed diesels. The centerline concentration is naturally a function of nozzle diameter, but it was found that they were not directly correlated, and thus the correction factor was altered.

$$C_c = \frac{0.75}{\frac{dR}{ds} KLA} d_N \sqrt{\frac{\mu \rho_f}{\rho_a}} \frac{1}{s} \qquad (1.12)$$

## 2.6 Rate of Heat Release and Pressure

All parameters are now in place to begin moving forward with the ROHR calculation. The assumption for combustion is that of a Simple Chemically Reacting System (SCRS). This means that the fuel mixed with air burns instantaneously. Upper and lower limits of equivalence ratio are imposed to determine when fuel is combustible, though this is a departure from SCRS. SCRS does not define an upper combustion limit,

but this must be defined for this model and is taken to be $\phi = 3.125$. This is the same limit as used in [1] and is very rich for local combustion. Such a rich upper limit is used to ensure all combustion is captured. A lower limit of $\phi = 0.1$ is also imposed.

The change in prepared fuel mass between the limits per change in penetration length can now be determined and is summarized as Equation (1.13). The prepared fuel mass is defined as the amount of fuel that has been prepared for combustion; this is the amount of fuel that is in the cylinder between the fuel concentration limits. The $\varepsilon$ values are calculated using (1.9) and the upper and lower burning equivalence ratios (and therefore concentrations) previously imposed. (1.13) is also naturally a function of the size of the jet plume and centerline fuel concentration.

$$C_c > C_{st} : \frac{dm_{fprep}}{ds} = C_c \rho_a KLA^2 2\pi R^2 \left( \int_{\varepsilon_{st}}^{\varepsilon_l} (1-\varepsilon^{1.5}) \varepsilon d\varepsilon + \int_{\varepsilon_u}^{\varepsilon_{st}} \lambda \left(1-\varepsilon^{1.5}\right) \varepsilon d\varepsilon \right) \quad (1.13)$$

The limits of integration refer to the dimensionless radii for upper, lower, and stoichiometric limits. λ is the air ratio and is a function of the cylinder fuel concentration determined by equation (1.12). In [1], a second equation was established for the change in prepared mass when the centerline concentration below the stoichiometric concentration. However, that was found to be inappropriate in the cases for which this simulation was developed. Once again, this can be attributed to the fact that [1] uses large bore, slow speed marine diesel engines for algorithm development. The higher speed, smaller bore engines analyzed in this work did not follow the second equation

provided in [1]. This is not arbitrary; the larger bore engines in [1] had ROHR curves much deeper into the expansion stroke, so the second equation provided by the authors in that case was not applicable to higher speed engines with shorter ROHR curves.

In order to convert equation (1.13) to a time resolved change in mass, a jet front equation is developed. This equation is a simple differentiation of (1.11) and is provided in [1].

$$u_F = \frac{0.572}{\frac{dR}{ds}KLA} u_0 d_N \sqrt{\frac{\mu\rho_f}{\rho_a}} \frac{1}{s} = \frac{ds}{dt} \tag{1.14}$$

$$\frac{dm_{fprep}}{dt} = \frac{dm_{fprep}}{ds} u_F \tag{1.15}$$

Equation (1.14) is posed in terms of variables that have previously been defined and is also equal to the change in penetration per time. This is the velocity of the jet front as it penetrates the chamber. Though this is essentially zero when impingement occurs, this is resolved by calculating ds/dt as a function of dR/ds and is constant as shown by equation (1.6). This prevents (1.14) from approaching zero upon impingement. Therefore, equation (1.14) can be used in conjunction with the change in prepared fuel mass per penetration length in (1.9) to determine the change in prepared fuel mass per unit time. With equations (1.14) and (1.15), the next step is to determine the overall change in mass between the combustion limits. During the injection duration, the change in mass between the limits is equal to the change in the prepared mass between the limits as defined by (1.16). After injection ends this method must change as there is no longer mass addition occurring. The change in mass now becomes the difference between the

mass burned during injection and the mass burned after injection to ensure that mass is conserved. This is seen in equation (1.17) and is now a function of the time after the end of injection and the mass in the chamber.

$$t \le t_{\text{inj end}} : \frac{dm_{\text{fbl}}(t)}{dt} = \frac{dm_{\text{fprep}}(t)}{dt} \tag{1.16}$$

$$t > t_{\text{inj end}} : \frac{dm_{\text{fbl}}(t)}{dt} = \frac{dm_{\text{fprep}}(t)}{dt} - \frac{dm_{\text{fprep}}(t - t_{\text{inj end}})}{dt} \tag{1.17}$$

Now that the change in mass per unit time has been determined, the ROHR can be calculated.

$$\frac{\delta Q}{\delta t} = \text{LHV}\frac{dm_{\text{fbl}}}{dt} \tag{1.18}$$

This is the end result for the use of the algorithm developed in [1] for this model. LHV is the lower heating value of the fuel.

Determining pressure from ROHR is relatively simple.

$$\frac{dP}{dt} = \frac{\gamma - 1}{V_c}\frac{\delta Q}{\delta t} - \gamma\frac{dV}{dt}\frac{P^{i-1}}{V_c} \tag{1.19}$$

In this equation (1.19), the instantaneous cylinder volume, $V_c$ must be known along with the volumetric rate of change with respect to time. Gamma is the ratio of specific heats, and was taken to be 1.35 in this work. This equation can be rearranged to solve for ROHR if a pressure profile is known.

## 2.7 Temperature

The models for temperatures of the zones and NO formation are presented in [2]. The NO prediction is very sensitive to temperature, so this is an extremely important aspect of the simulation. The burned zone temperature is a function of the total number of moles in the cylinder, the global temperature, the number of burned moles, and the unburned zone temperature.

The number of global moles is calculated using the ideal gas law, where the temperature, pressure, and volume used are taken at the beginning of injection. These are shown as $T_0$, $p_0$, and $V_0$, respectively in (2.1).

$$n_g = \frac{p_0 V_0}{\bar{R} T_0} \tag{2.1}$$

The gas constant, R, used in (2.2) is the universal gas constant. The total number of moles in the cylinder is assumed to be constant throughout the combustion process. Pressure, p, and volume, V, in (2.2) are the instantaneously calculated pressure and volume. The pressure is found using the predicted ROHR curve.

$$T_g = \frac{pV}{n_g \bar{R}} \tag{2.2}$$

The ratio of specific heats, γ, in (2.3) is assumed to be constant in the unburned zone. This is a good assumption because the unburned zone temperature remains

relatively low throughout combustion. $T_{g0}$ and $P_{g0}$ are the temperature and pressure at the start of injection, respectively. As before, p is the cylinder pressure as calculated from the predicted ROHR.

$$T_{uz} = T_{g0}\left(\frac{p}{p_{g0}}\right)^{\frac{\gamma-1}{\gamma}} \tag{2.3}$$

$$n_{bz} = \frac{Q}{LHV \cdot M_f}\left(1+\frac{M_f \lambda AF_s}{M_a}\right) \tag{2.4}$$

Equation (2.4) computes the number of moles in the burned zone. $Q$ is computed from the integration of (1.13). $M_f$ and $M_a$ are the molar masses of fuel and air, respectively. $AF_s$ is the stoichiometric air/fuel ratio. Interestingly, λ is taken to be constant here. While λ can easily be calculated using the methods described in [1], a constant value provided consistently reasonable results in this simulation. $\lambda = 1.3$ is the value used in the calculation of (2.4).

Equation (2.5) shows the burned zone temperature in the cylinder. The variables represent the number of moles, n, and temperatures, T, in each zone. The subscripts g, uz, and bz refer to global, unburned zone, and burned zone.

$$T_{bz} = \frac{n_g T_g - (n_g - n_{bz})T_{uz}}{n_{bz}} \tag{2.5}$$

## 2.8 Equilibrium and NO Calculation

To accurately determine the NO produced, a clear picture of the burned zone composition must be obtained. Based on the λ obtained from the ROHR calculations and $T_{bz}$, equilibrium composition can be determined. Two equilibrium reactions are used.

$$H_2O \leftrightarrow H_2 + \frac{1}{2}O_2 \quad (3.1)$$

$$CO_2 \leftrightarrow \frac{1}{2}O_2 + CO \quad (3.2)$$

Equations (3.1) and (3.2) are used to determine equilibrium compositions for $CO_2$, $H_2O$, $N_2$, $O_2$, CO, and $H_2$. Additionally, EGR was also taken into account for determination of equilibrium concentrations of the aforementioned molecules. This was accomplished assuming an EGR composition profile. The simulation was run without EGR for various cases, and the exhaust concentrations were analyzed to determine a reasonable EGR composition. Using this, determining the initial composition was possible. With a given EGR rate, the atom balances could be modified to include the elemental compositions of EGR. Based on these and the global number of moles from (2.1), concentrations of all can be determined for use in the following equations. The "c" values describe concentrations, and the "e" superscript on concentration values denotes equilibrium concentrations in (3.4), (3.6), and (3.7). The temperatures used in the same equations are all those of the burned zone as calculated by (2.5).

$$O_2 \leftrightarrow O + O \tag{3.3}$$

$$c_O^e = \frac{3.6 \cdot 10^3 e^{\frac{-31090}{T_{bz}}} \sqrt{c_{O_2}^e}}{\sqrt{RT_{bz}}} \tag{3.4}$$

$$O_2 + N_2 \leftrightarrow 2NO \tag{3.5}$$

$$c_{NO}^e = \sqrt{20.3 e^{\frac{-21650}{T_{bz}}} c_{O_2}^e c_{N_2}^e} \tag{3.6}$$

Equations (3.3)-(3.6) are used for determination of equilibrium concentrations for use in equation (3.7).

$$\frac{\partial c_{NO}}{\partial t} = \frac{15.2 \cdot 10^{13} e^{\frac{-38000}{T_{bz}}} c_O^e c_{N_2}^e \left(1 - \left(\frac{c_{NO}}{c_{NO}^e}\right)^2\right)}{1 + \frac{7.6 \cdot 10^{13} e^{\frac{-38000}{T_{bz}}} c_O^e c_{N_2}^e}{1.5 \cdot 10^9 e^{\frac{-19500}{T_{bz}}} c_{NO}^e c_O^e} \left(\frac{c_{NO}}{c_{NO}^e}\right)} \tag{3.7}$$

Equation (3.7) above is representative of the three step Zeldovich mechanism. However, it was noted in [2] that (3.7) is not valid if the volume of the zone to which it is applied is changing. Since the burned zone volume does change, another equation is introduced to account for this variance.

$$\frac{dc_{NO}}{dt} = \frac{\partial c_{NO}}{\partial t} - \frac{c_{NO}}{V} \frac{dV}{dt} \tag{3.8}$$

The volumetric terms in (3.8) are for the burned zone only. The burned zone volume (and rate of change) can be determined using ideal gas law and the number of burned zone moles. This expresses the rate of change of NO concentration. After integration of (3.8), the mole fraction can be obtained.

$$X_{NO} = \frac{V_{bz} c_{NO}}{n_g} \qquad (3.9)$$

With the establishment of (3.9), the simulation is completed. To return the mole fraction in parts per million (as is common for NO reporting), (3.9) only needs be multiplied by $10^6$.

**2.9 Expansion and Exhaust**

Expansion is computed similarly to compression in that a polytropic relation is used. It relies only on pressure at the previous crank angle, volume at the current and previous crank angle, and the polytropic exponent. Exhaust pressure is assumed to decrease linearly until the manifold pressure is reached. This does not intuitively sound correct, but for all cases the experimental and predicted pressure matched well in this area. However, this is a non-critical step in the process, so a high degree of resolution is not necessary. Therefore, this method is acceptable.

## 2.10 Performance Parameters

As previously noted, the friction model used for determination of BMEP from IMEP was the Heywood-Sandoval model from [12]. This is detailed by the following equations.

$$IMEP = \frac{W_{cycle}}{V_d} \tag{4.1}$$

The IMEP is simply the work done in the cycle divided by the displaced volume.

$$PMEP = 0.178 \cdot (\frac{P_{in} S_m}{P_{atm}})^2 + 3.00e-3 \cdot (\frac{S_m}{n_v r_e^4}) \tag{4.2}$$

PMEP is shown in (4.2). It is a function of intake and atmospheric pressure. $S_m$ is the instantaneous piston speed, $n_v$ is the number of valves per cylinder, and $r_e$ is the ratio of the exhaust valve diameter to stroke.

$$CFMEP = 1.22e5 \cdot \frac{D_b}{B^2 L n_c} + 3.03e-4 \cdot \frac{N D_b^3 L_b n_b}{B\ L n_c} + 1.35e-10 \cdot \frac{N D_b n_b}{n_c} \tag{4.3}$$

CFMEP becomes more complex. It is a function of bore and stroke, as well as engine speed. It is also a function of the number of cylinder and bearings, $n_c$ and $n_b$ which are equal in the engines analyzed here. Finally, the bearing diameter, $D_b$ is also taken into account.

$$RFMEP = 2.94e2 \cdot \frac{S_m}{B} + 4.06e4 \cdot (1 + \frac{1000}{N}) \cdot (\frac{1}{B^2}) + 3.03e-4 \cdot \frac{ND_b^3 L_b n_b}{B^2 L n_c} \quad (4.4)$$

RFMEP sums the rotating friction of the engine. It is therefore a function of instantaneous piston speed, bore, engine speed, bearing diameter, the number of cylinders, stroke, and the bearing length, $L_b$.

$$RFMEP_{gas} = 6.89 \cdot \frac{P_{in}}{P_{atm}} \cdot (0.088R_c + 0.182R_c^{(1.33-1.4e-2 \cdot S_m)}) \quad (4.5)$$

(4.5) shows RFMEP with gas pressure loading taken into account. It is a function of intake and atmospheric pressure, instantaneous piston speed, and the compression ratio, $R_c$.

$$AFMEP = 8.32 + 1.83e-3 \cdot N - 7.45e-7 \cdot N^2 \quad (4.6)$$

AFMEP measures the loss from auxiliary sources. It is developed to only be a function of engine speed.

$$VFMEP = 244 \frac{Nn_b}{B^2 L n_c} + C_{ff}(1 + \frac{1000}{N})(\frac{n_v}{L n_c}) + C_{rf} \frac{N n_v}{L n_c} + C_{oh} \frac{L_v^{1.5} N^{0.5} n_v}{B L n_c} + C_{om}(1 + \frac{1000}{N})(\frac{L_v n_v}{L n_c}) + 4.12 \quad (4.7)$$

VFMEP is the final piece before calculating the TFMEP. It is a function of engine speed, number of bearings/cylinders, bore, the number of valves per cylinder, the maximum valve lift $L_v$, and a series of coefficients that are given by [12] and found in the table below.

$$TFMEP = CFMEP + RFMEP + AFMEP + PMEP + VFMEP + RFMEP_{gas} \quad (4.8)$$

$$BMEP = IMEP - TFMEP \quad (4.9)$$

The TFMEP is the sum of equations (4.2-4.7). The BMEP is the difference between the IMEP and TFMEP. This is the value of interest.

**Table 5 - Friction coefficients from [12].**

| **Coefficient** | **Value** |
|---|---|
| $C_{ff}$ | 600 |
| $C_{rf}$ | 0.0227 |
| $C_{oh}$ | 0.2 |
| $C_{om}$ | 42.8 |

# 3. RESULTS AND DISCUSSION

The predicted pressure curves, in comparison to experimentally-based pressure curves, are shown below in figures 4-12.

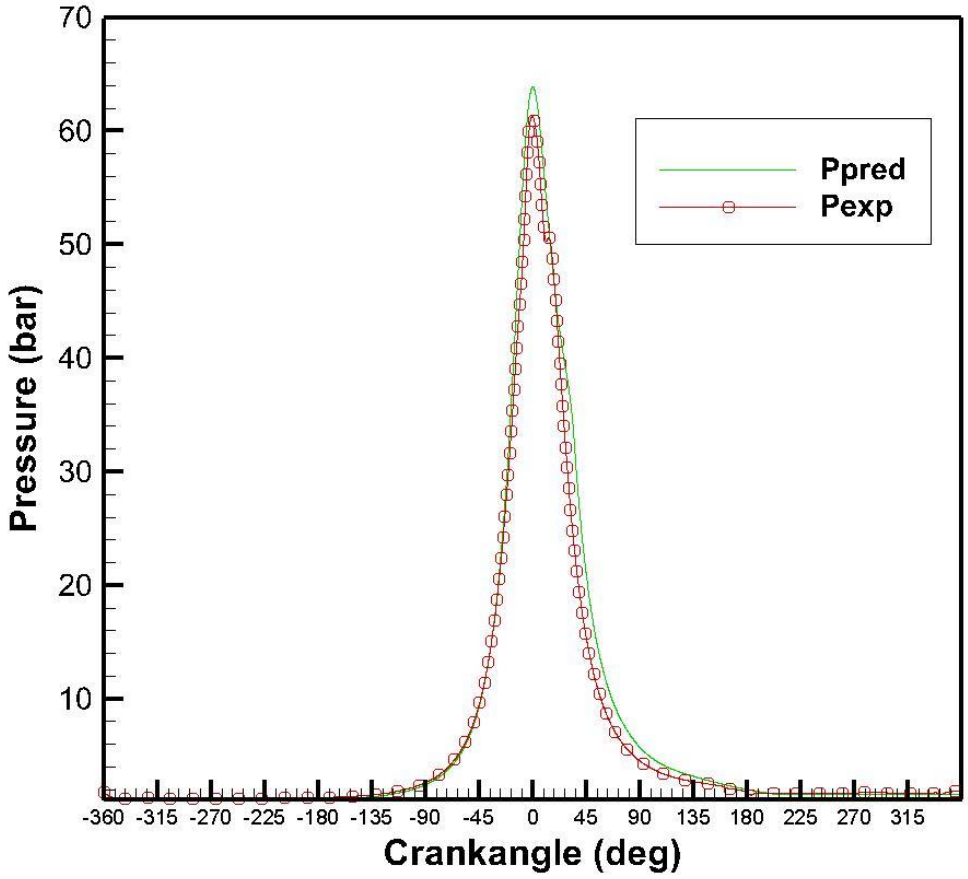


**Figure 4 - Predicted and experimental pressure for M1.**

The prediction for M1 matches fairly well with the experimental pressure curve. There is a pilot injection for this case, but the main injection is relatively early and is therefore easily captured.

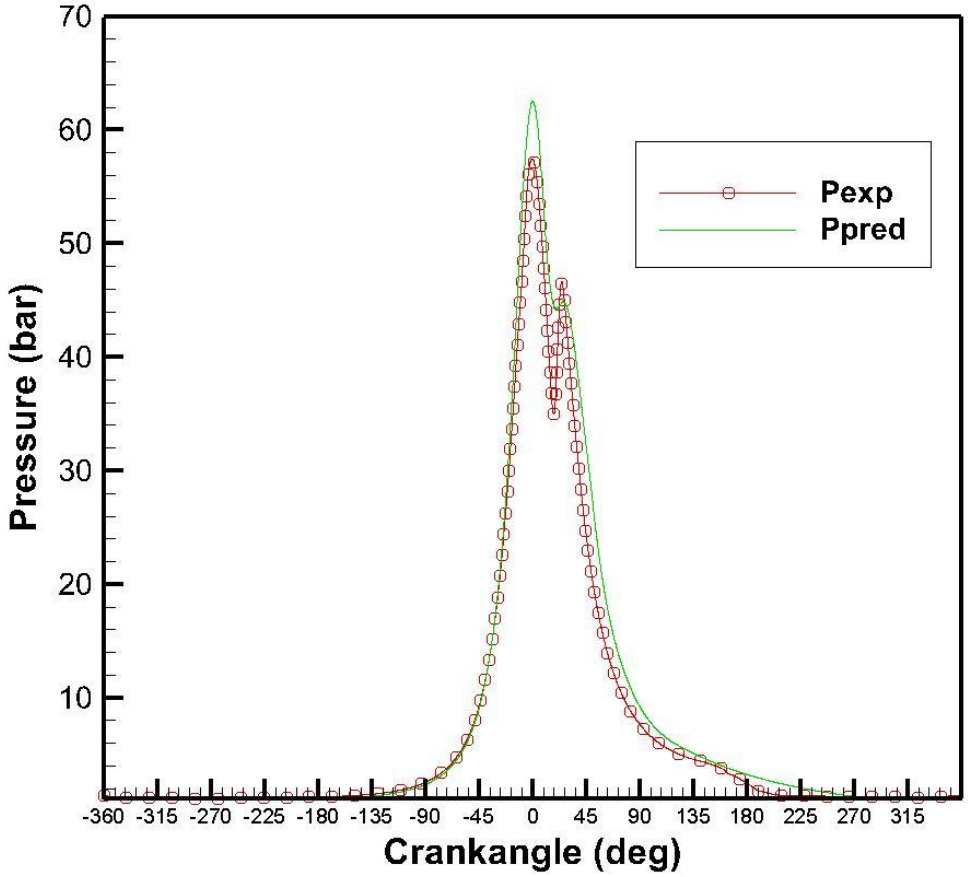


**Figure 5 – Predicted and experimental pressure for M2.**

M2 is captured reasonably well, especially since there is a very early pilot injection, and the main injection occurs later. This was compensated for with an imposed injection timing that was between the pilot and main injection, but accuracy suffered as a result.

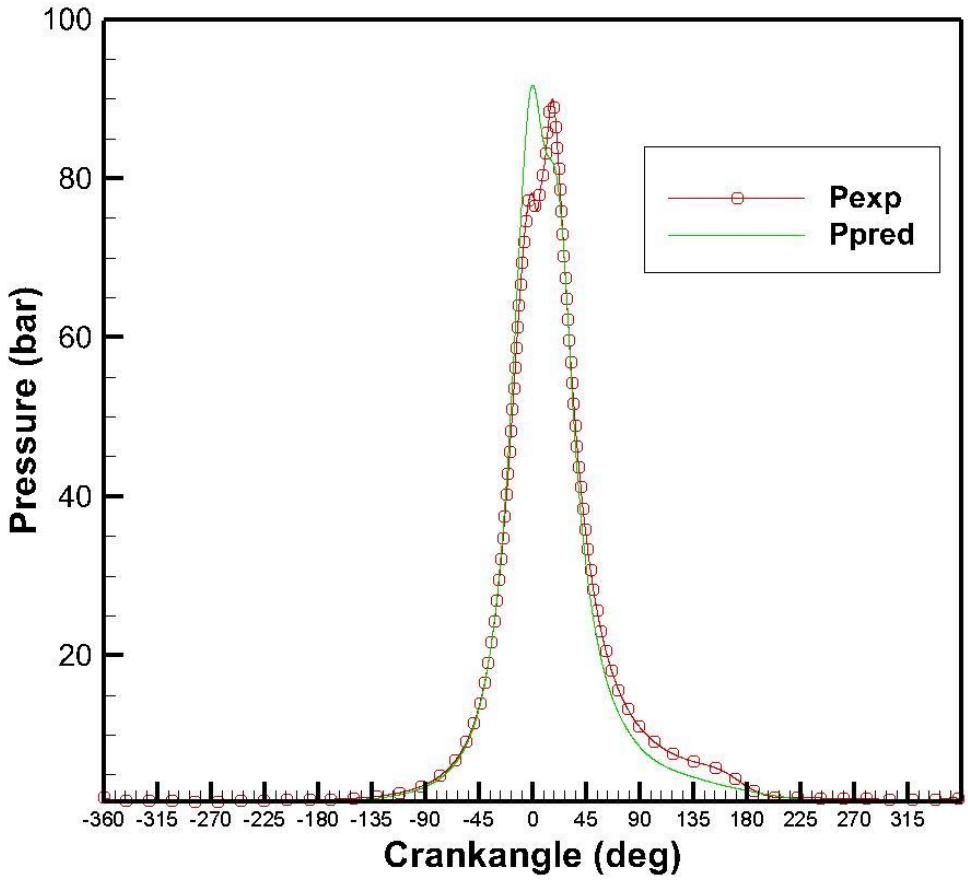


**Figure 6 – Predicted and experimental pressure for M3.**

In this full load, low speed case, the premixed burn is not well captured. While the peak values are similar, the prediction shows the maximum pressure happening much sooner. This is a result of not using an ignition delay correlation, and assuming all burning is uniform.

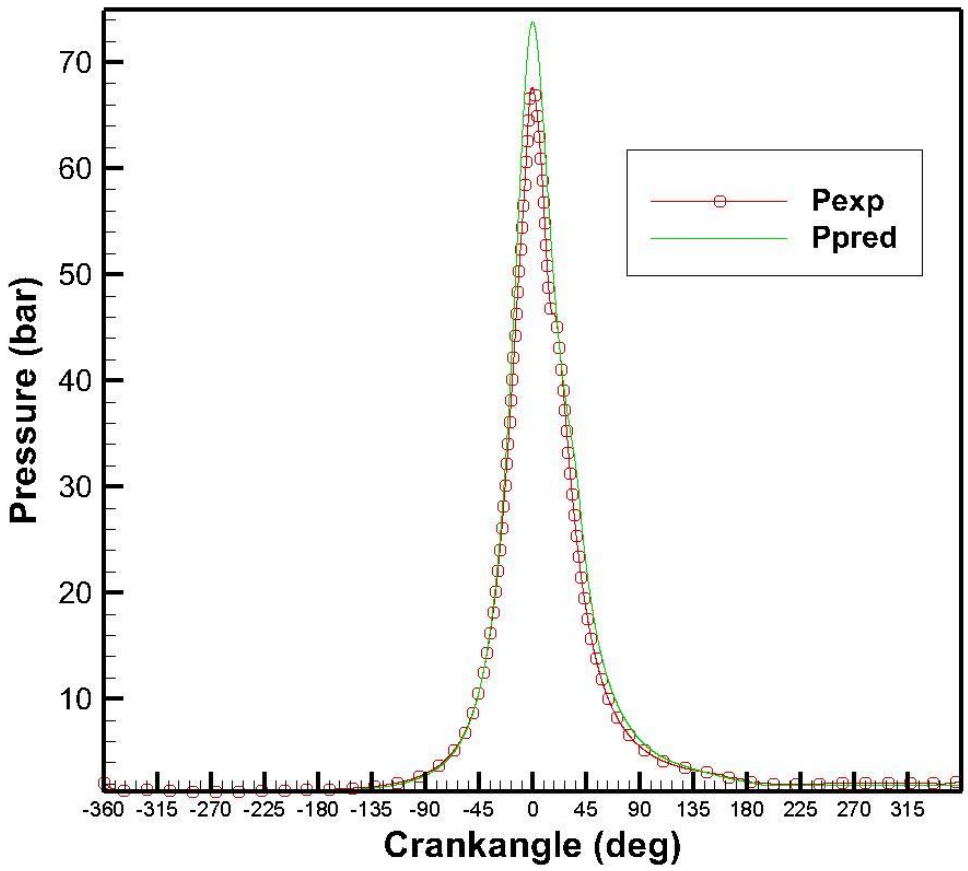


**Figure 7 – Predicted and experimental pressure for M4.**

As with M1, the simulation is not as proficient at capturing multiple injections. As a result, over prediction of pressure is expected.

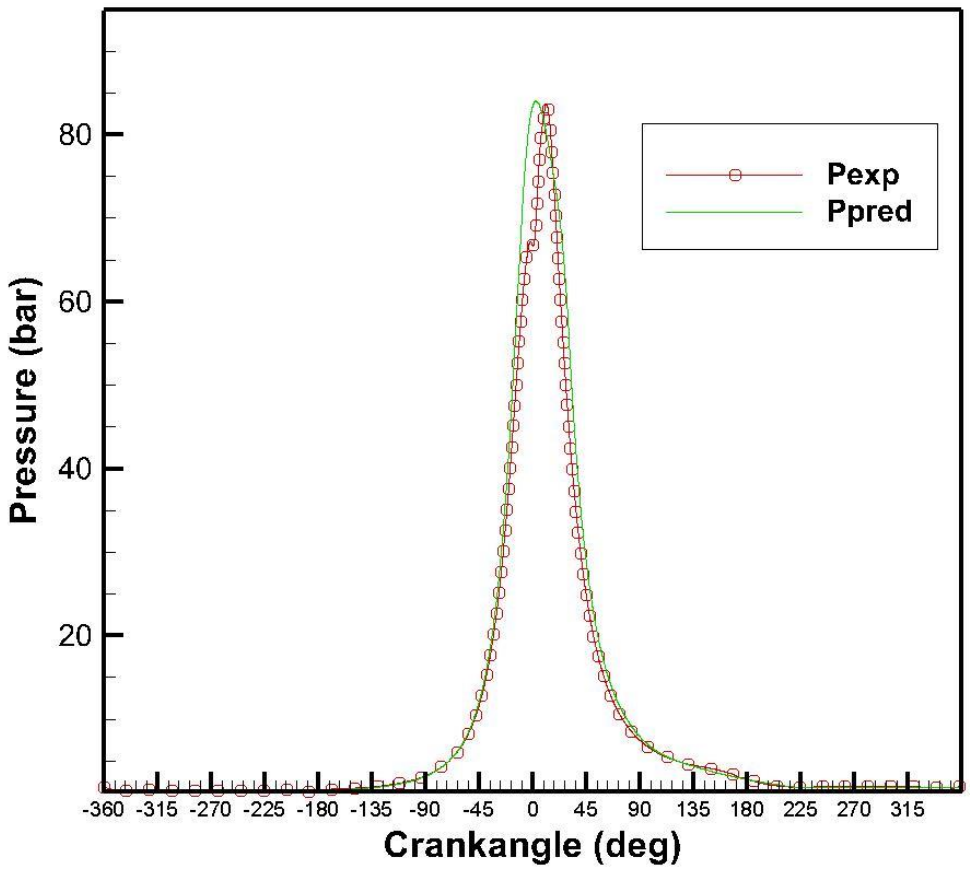


**Figure 8 - Predicted and experimental pressure for M5.**

Medium load cases are predicted well and the peak pressure for experimental and predicted pressures are very close. However, the loss of the premixed spike means that while the pressure peak value is similar to the experimental, its location changes.

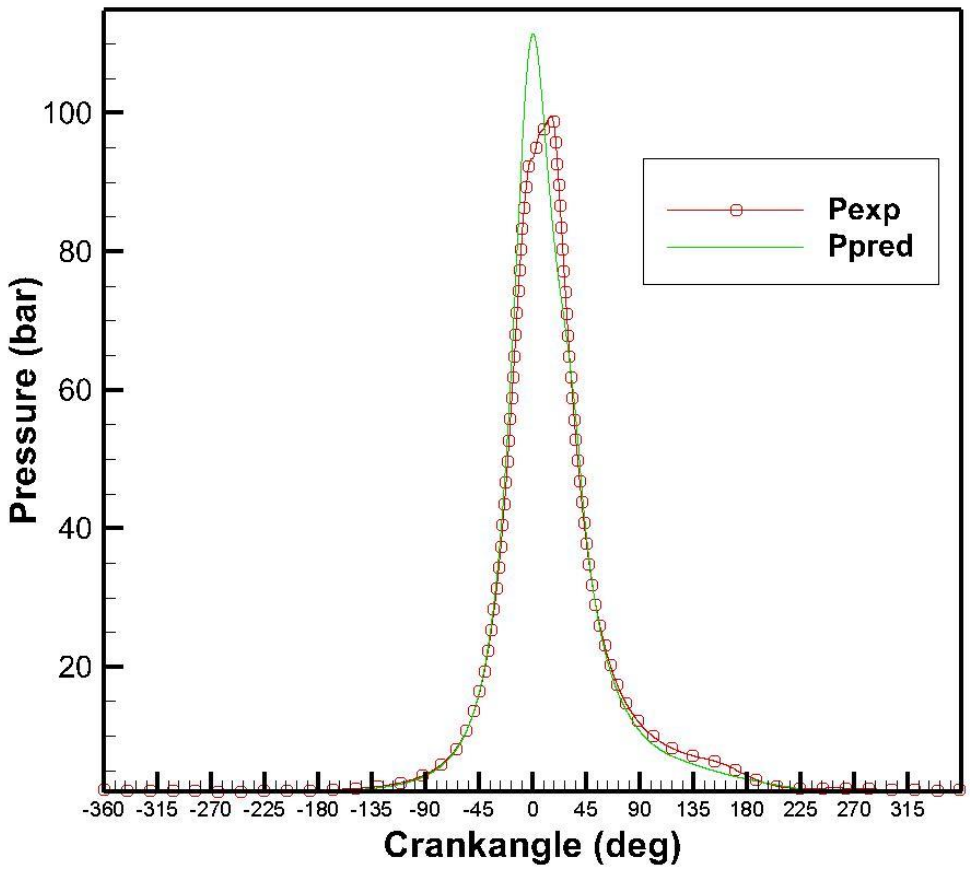


**Figure 9 - Predicted and experimental pressure for M6.**

M6 is not well captured, and the full load case over predicts pressure significantly. Again, the lack of a premixed spike harms the simulation.

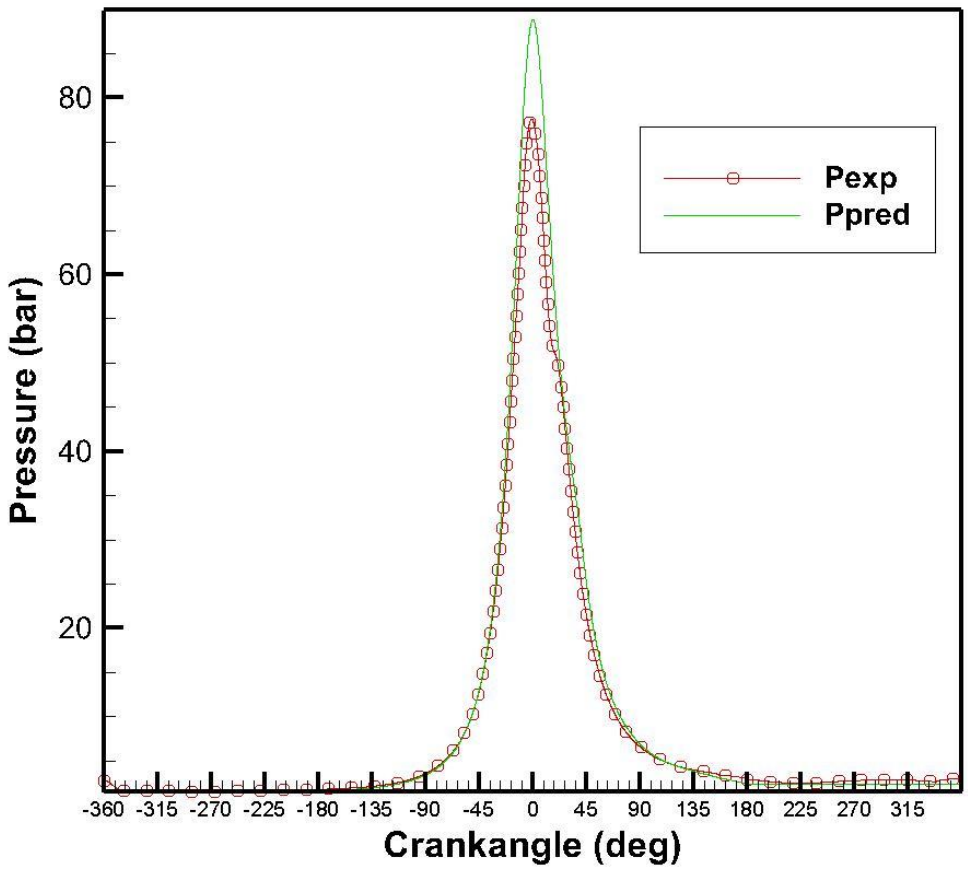


**Figure 10 - Predicted and experimental pressure for M7.**

M7 is a low load multiple injection case. It is not well captured as a result, and the prediction is much higher than experimental.

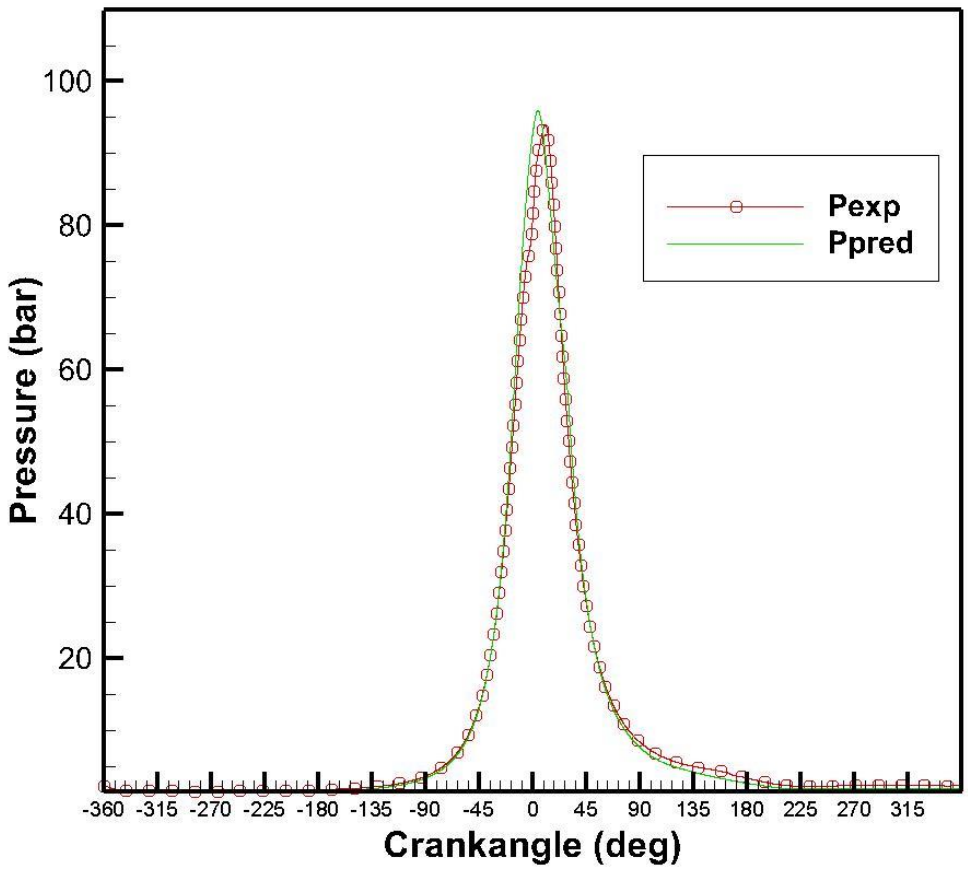


**Figure 11 - Predicted and experimental pressure for M8.**

M8 looks significantly better than M7. Medium load cases work well with this simulation, and the lack of a pilot injection also helps. This case uses a significant amount of EGR, and is still well captured.

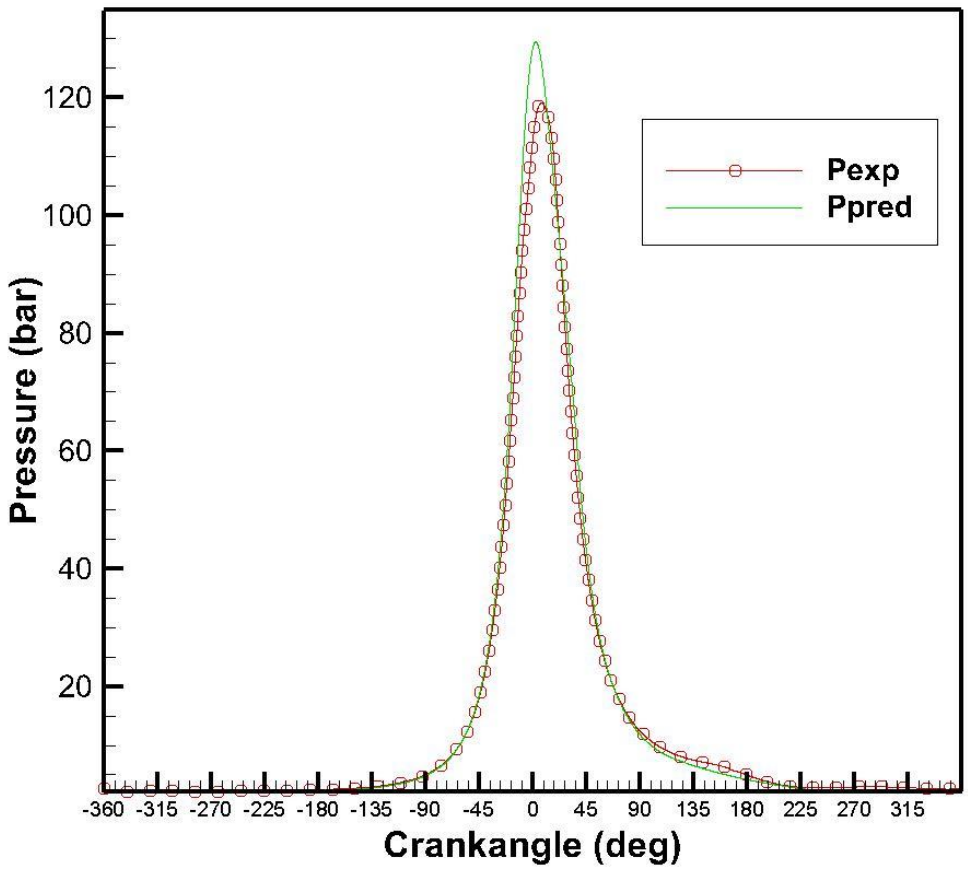


**Figure 12 - Predicted and experimental pressure for M9.**

M9 is again a high load condition. The simulation was developed to capture the widest range of cases possible, so high and low load cases suffer. Medium load, as demonstrated, is very accurate. This means that for many operating conditions, this method of simulation is proven accurate.

The calculated peak pressures are generally too high, but this does not lead to a large amount of inaccuracy of NO predictions as will be shown. The predicted pressures during compression match well with the experimental pressures, validating the method used for calculating compression pressure. Modes 1, 2, 4, and 7 include a pilot injection, and as a result the predicted pressures are significantly higher than the experimental. The method of calculating the rate of injection was shared among all 9 cases, so this naturally caused issues. The start of injection was taken to be the start of the pilot injection, and the break between pilot and main injection was not accounted for. This lends itself to higher peak pressures. An attempt was made to perform two separate ROHR calculations for each injection, but the predictions were erratic and did not reflect reality. Since most of the cases were reasonable without the need to do this, that particular approach was abandoned for this work. These cases will be further analyzed in regards to NO and temperature to determine the effects of calculating the injection duration as a single pulse later. As mentioned, the peak pressures were generally too high. As a result, the IMEP values did not match very well and generally over predicted. Mode 2 was also a particularly difficult mode for which to ascertain an accurate prediction. The three lower speed cases (modes 1-3) tended to be less accurate than the medium and higher speed cases in terms of NO prediction, and this is also reflected in the pressure prediction. This is likely due to the injection timings being closer to top dead center as opposed to the more advanced timings the other modes (besides 4) had. The injection timing for mode 2 is actually taken to be four degrees after top dead center, and this causes issues as the KLA factor was determined using modes with only timings before top dead center. This

timing was chosen because as a multiple injection case, it was difficult to pinpoint an accurate imposed timing. The pilot injection in M2 was early, and the start of the main injection was late. Since multiple injections could not be accurately modeled within the scope of this simulation, a large source of error is introduced for this mode. However, the main objective of this work is not to accurately predict ROHR or pressure, but rather NO. From Figures 4-12, IMEP was calculated and compared to the experimental values. The friction model from [12] is the suggested method for BMEP determination.

**Table 6 - Predicted and experimental IMEP for each operating case.**

| **Case** | **IMEP experimental (bar)** | **IMEP predicted (bar)** | **Percent error** |
|---|---|---|---|
| 1 | 3.04 | 5.563 | 45.32 |
| 2 | 7.59 | 10.34 | 26.52 |
| 3 | 12.3 | 9.835 | 24.82 |
| 4 | 3.53 | 5.165 | 31.58 |
| 5 | 7.74 | 9.222 | 16.05 |
| 6 | 12.6 | 11.17 | 12.68 |
| 7 | 3.61 | 5.165 | 30.14 |
| 8 | 8.20 | 8.322 | 1.474 |
| 9 | 12.7 | 13.14 | 2.847 |

As expected from the pressure curves, the predicted IMEP values are generally higher than the experimental IMEP values. This is due to the higher predicted peak pressures compared to the experimental peak pressures. The error numbers appear to be large, resulting in relative errors as high as 45%.This is an area that requires more work in future work to ensure that the predictions more closely match the experimental values.

Using the described methods, the burned zone temperatures for each case are provided below in figures 13-21. The red dashed line indicates the experimental NO values.

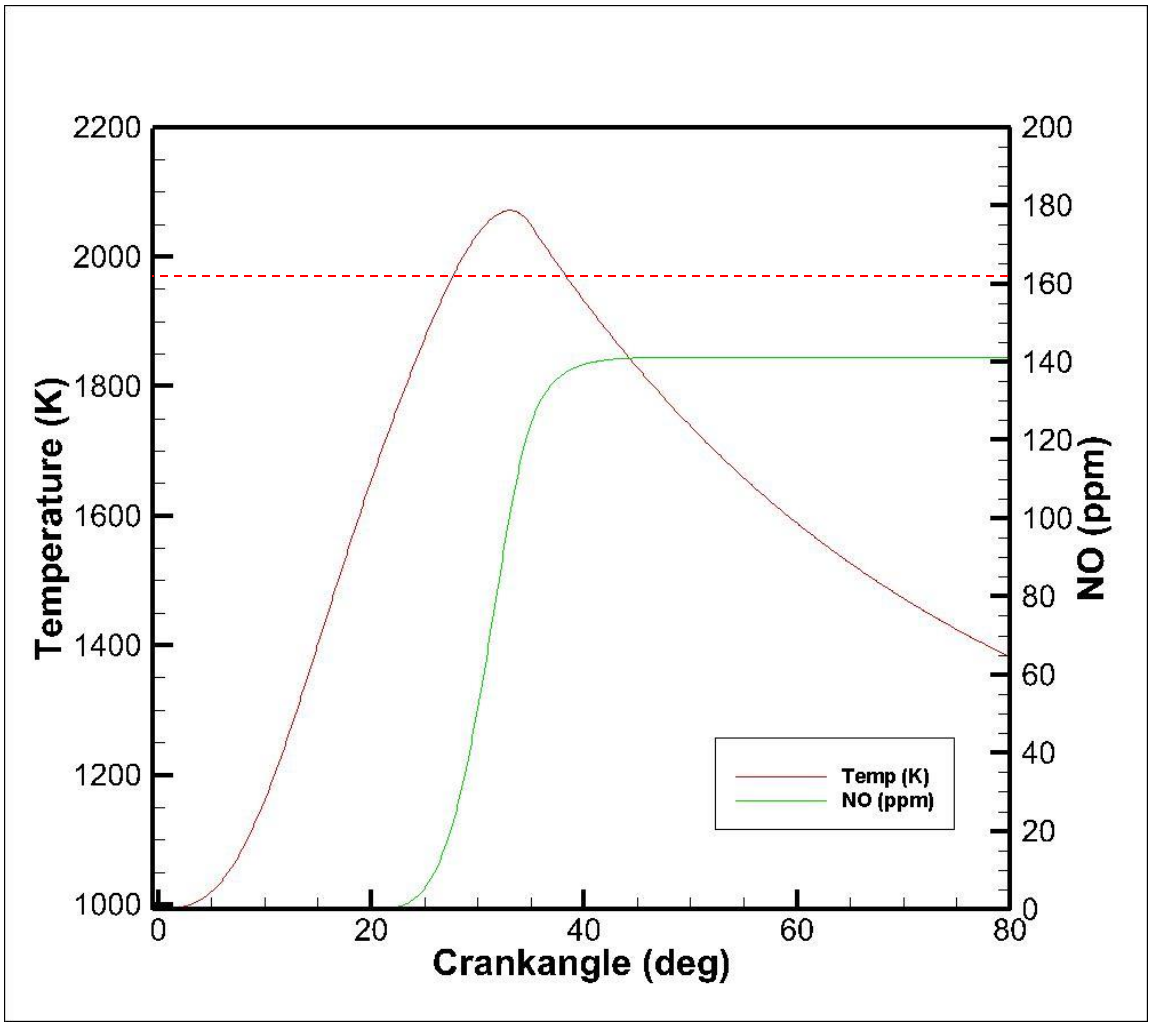


**Figure 13 - Burned zone temperature and NO fraction for M1.**

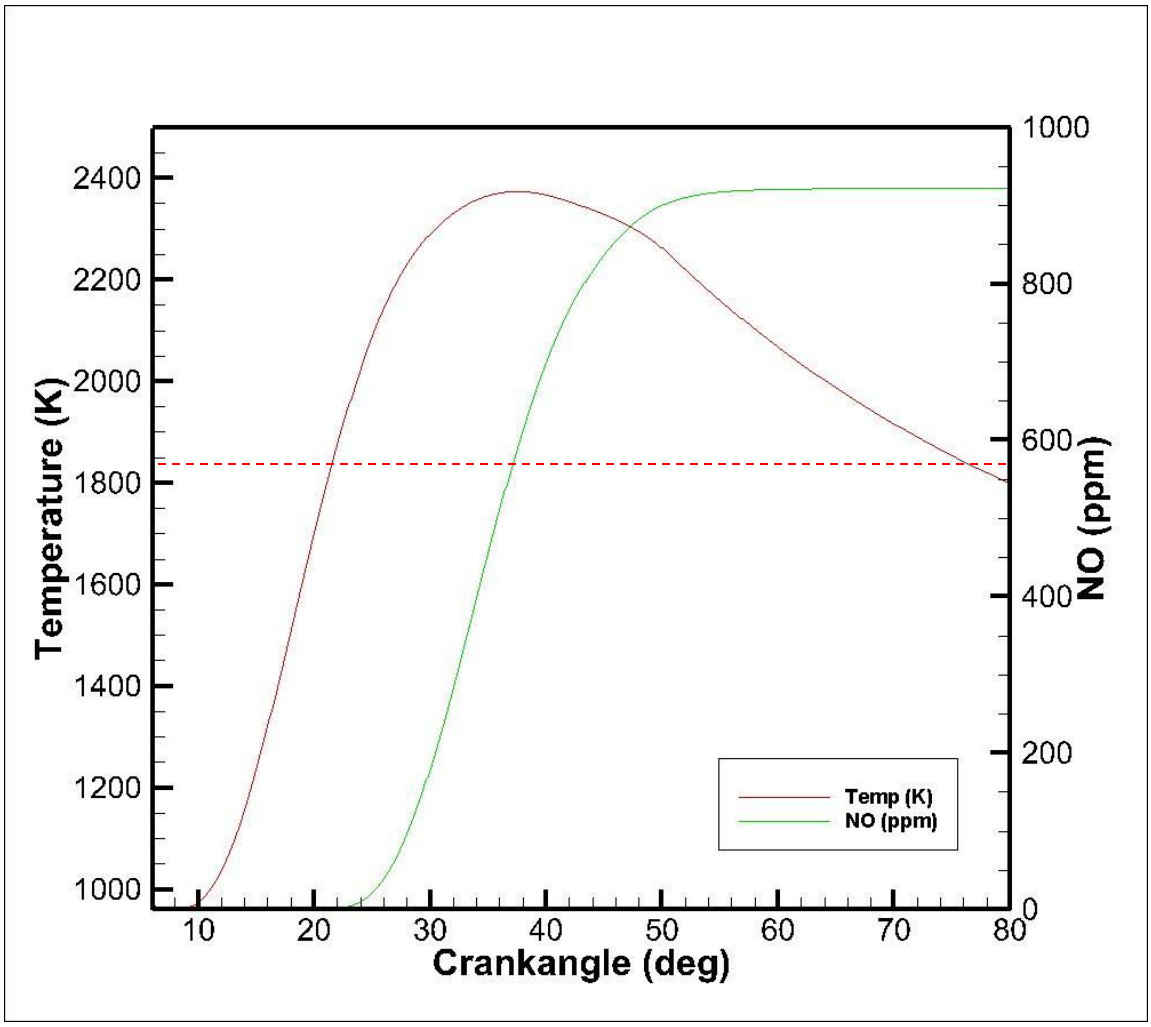


**Figure 14 - Burned zone temperature and NO fraction for M2.**

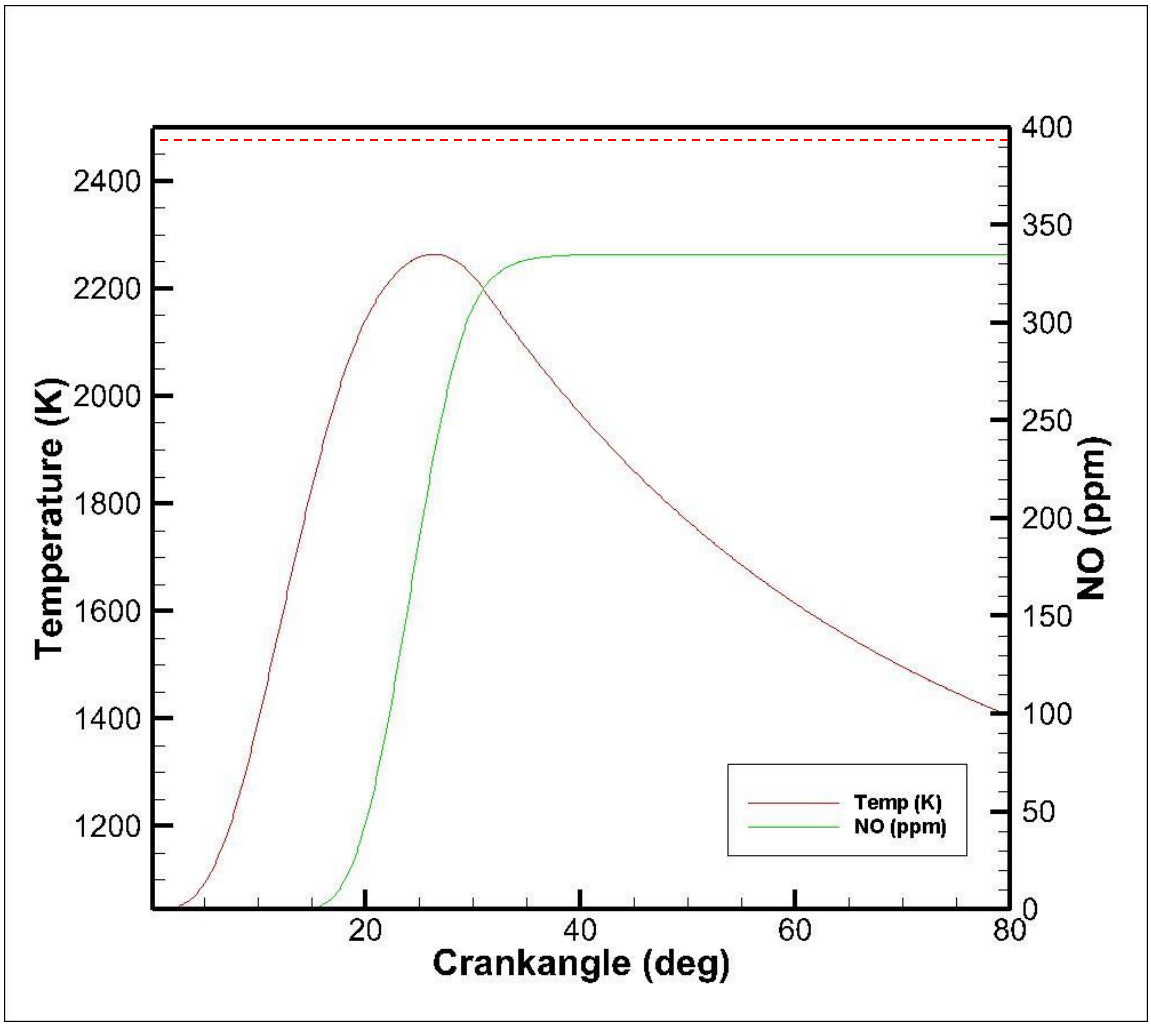


**Figure 15 - Burned zone temperature and NO fraction for M3.**

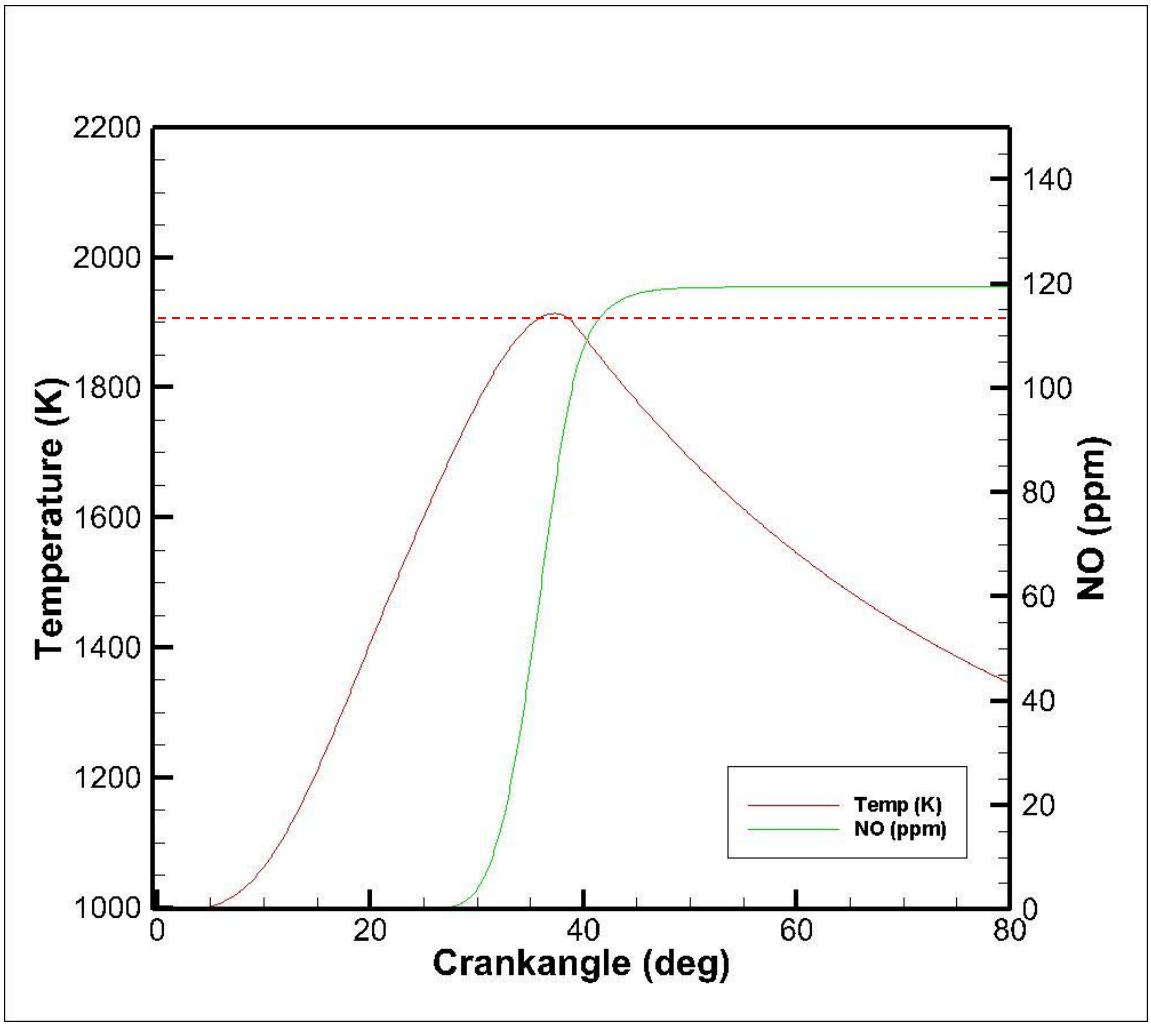


**Figure 16 - Burned zone temperature and NO fraction for M4.**

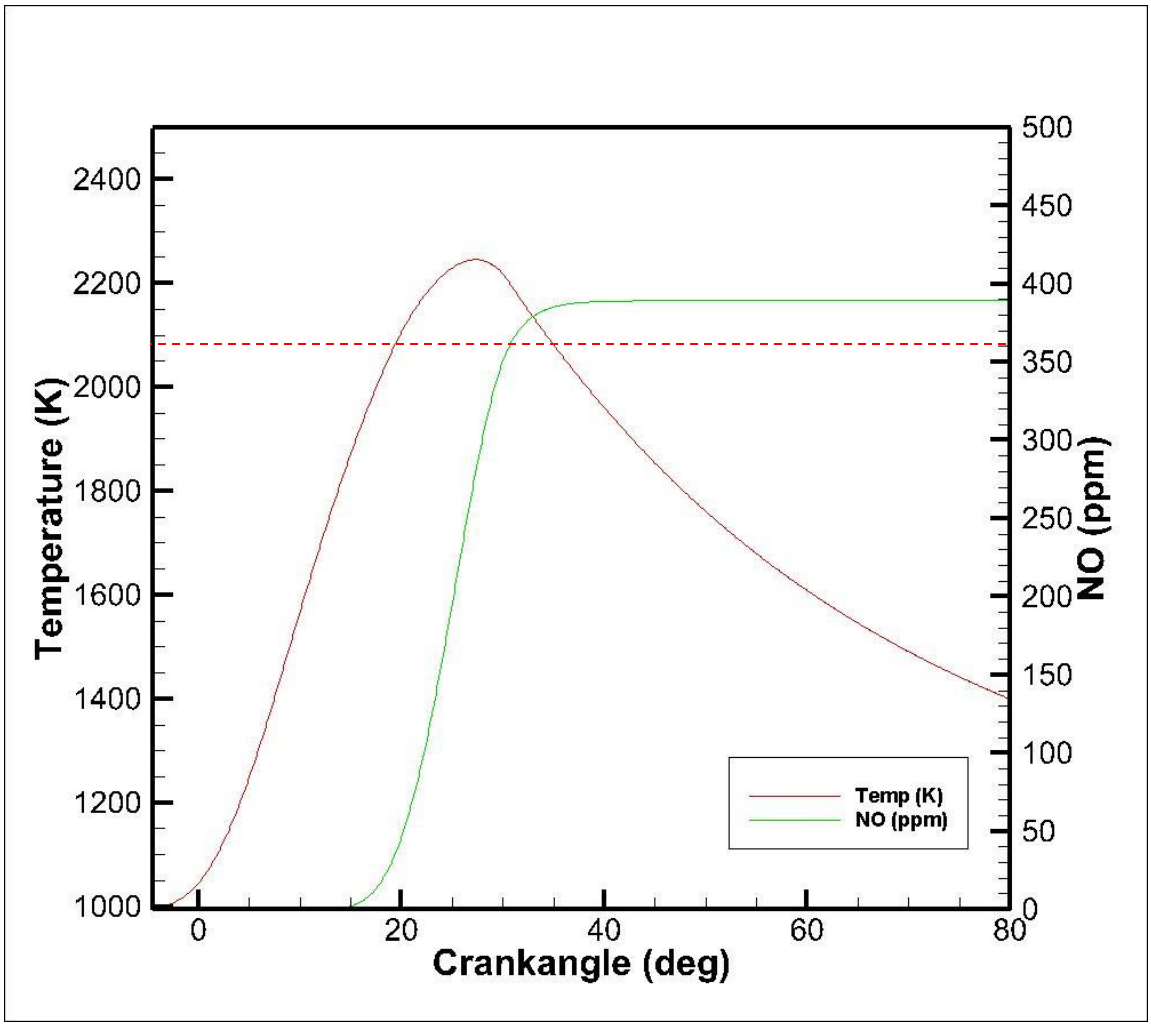


**Figure 17 - Burned zone temperature and NO fraction for M5.**

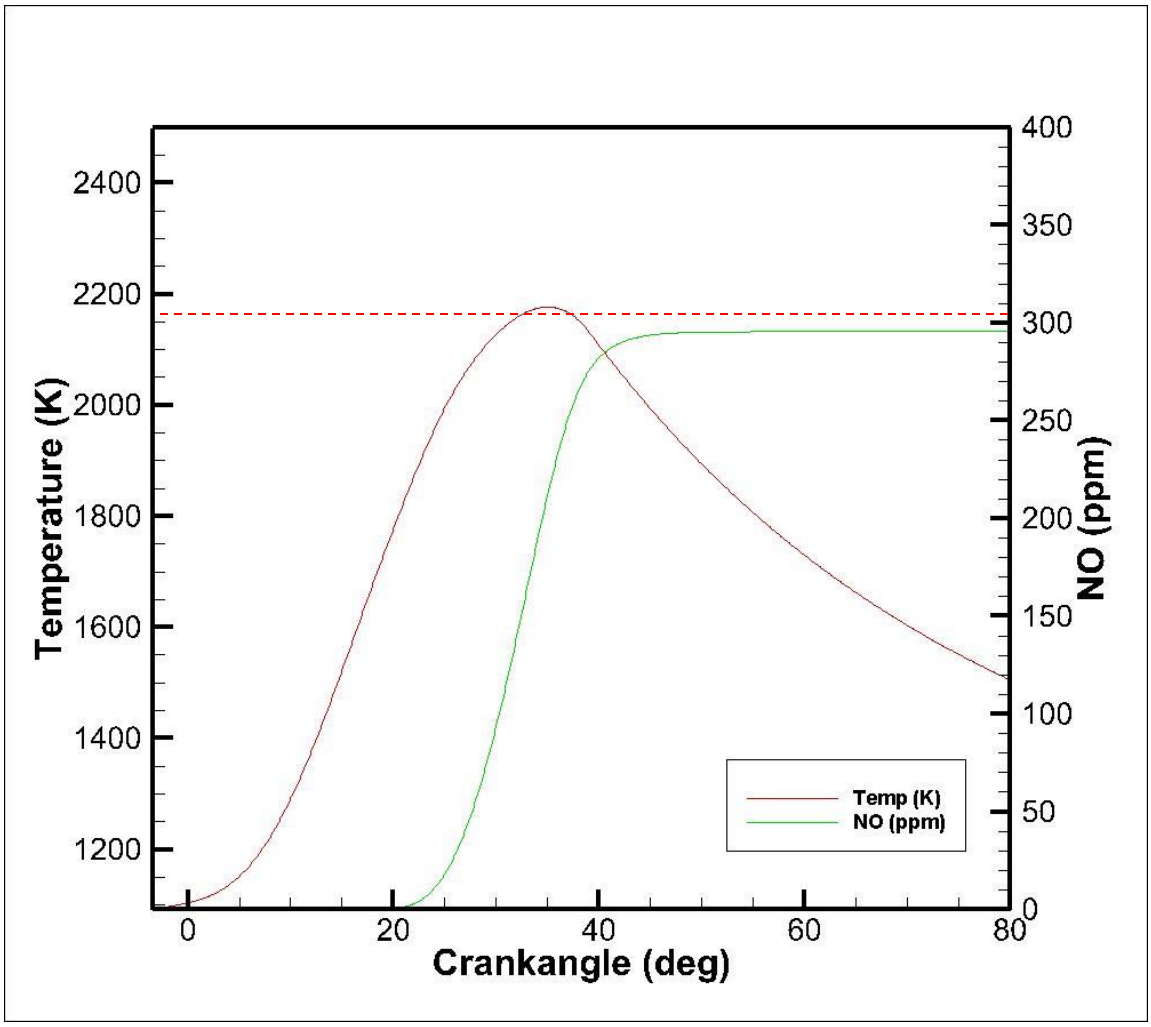


**Figure 18 - Burned zone temperature and NO fraction for M6.**

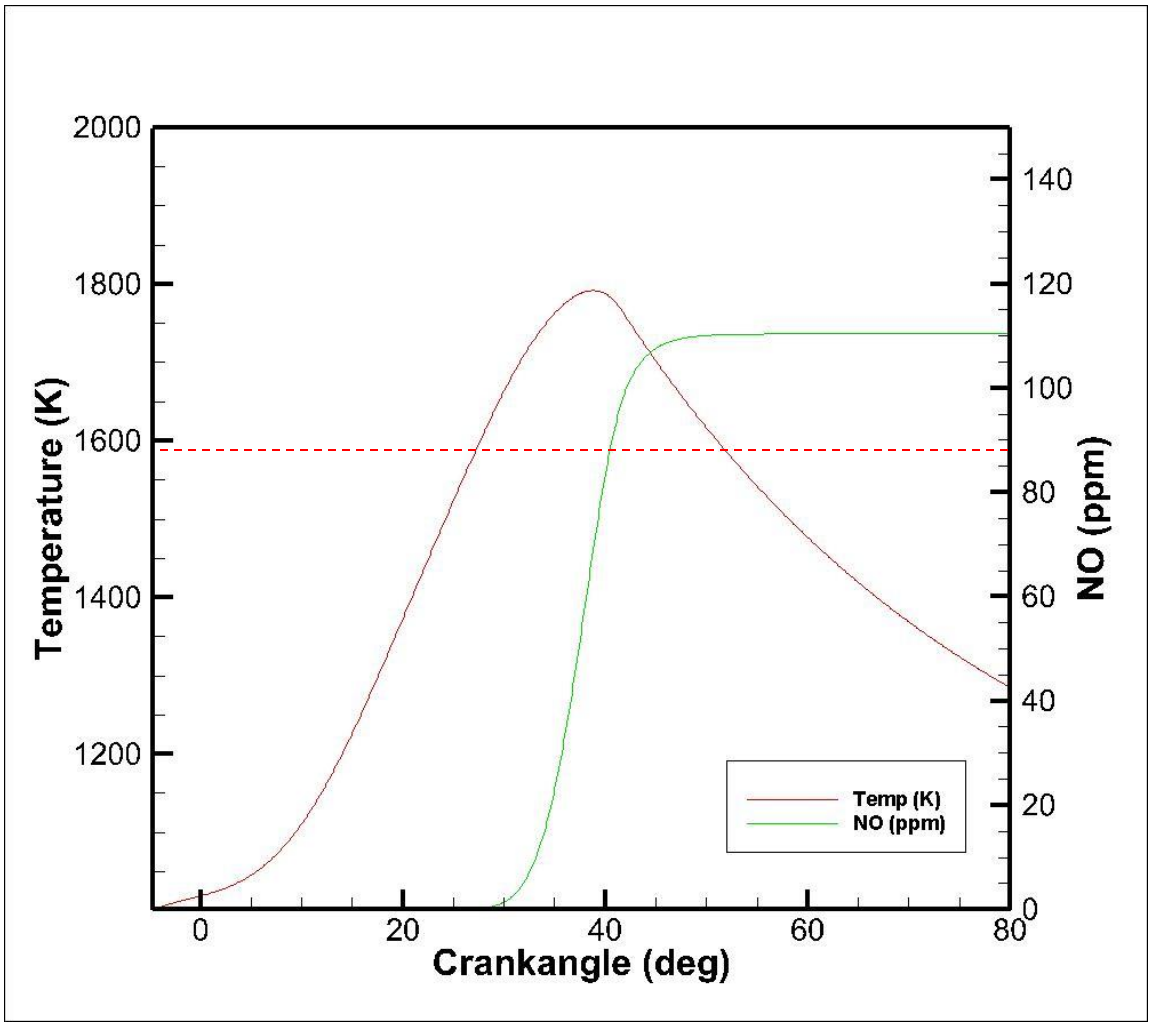


**Figure 19 - Burned zone temperature and NO fraction for M7.**

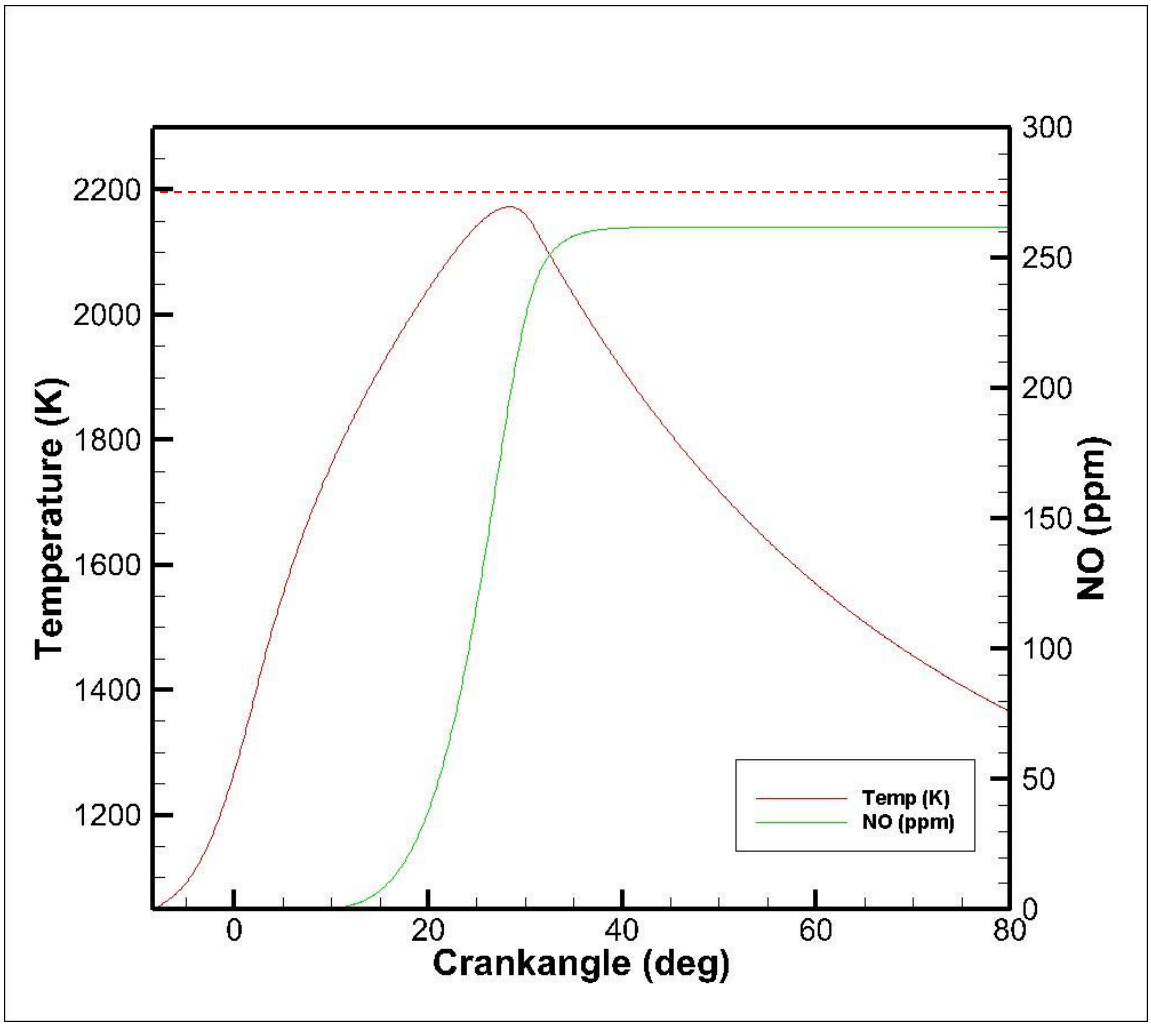


**Figure 20 - Burned zone temperature and NO fraction for M8.**

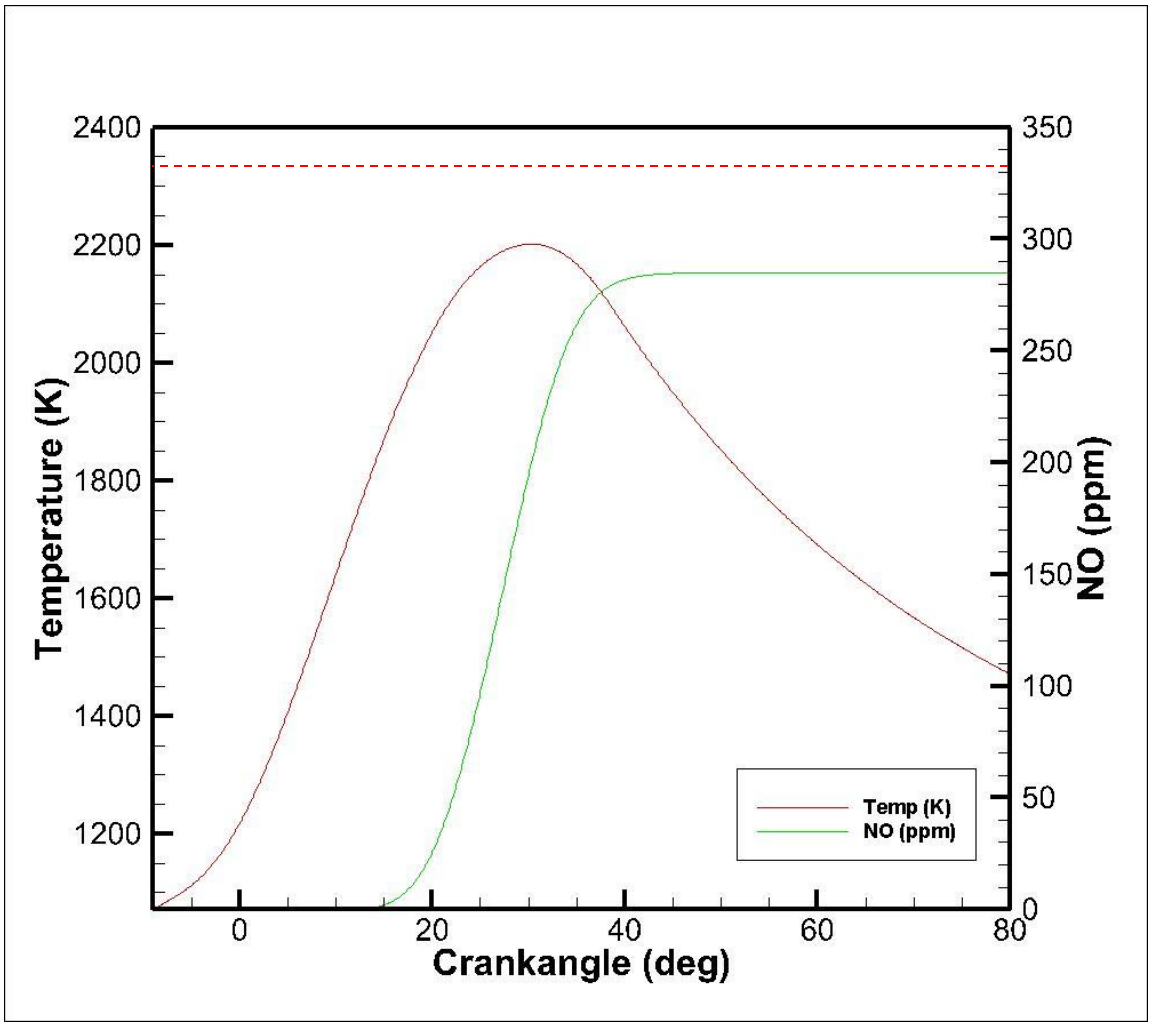


**Figure 21 - Burned zone temperature and NO fraction for M9.**

There is much that can be gleaned from figures 13-21. The first observation is that the cases that exhibit a higher total NO show higher burned zone temperatures. This is to be expected; it is only the first step in validation of the prediction algorithm. This is a common sense check that allows further analysis. The next area of interest is the rate at

which the NO formation occurs. For the cases with sharp temperature peaks, the rate increases rapidly. Cases with a more gently sloped temperature profile show NO formation rate to be equally gently sloped as compared with the steeper curves of others. Modes 8 and 9 are good examples of this behavior: while mode 8 shows a sharper temperature peak and therefore faster NO formation rate, mode 9 shows softer temperature peak and slower NO formation rate. For all cases, NO formation rate has the steepest slope at the peak temperature as expected. Low load cases (1, 4, and 7) show lower peak temperatures as compared to medium and high load cases. As previously noted, mode 2 has an injection timing much later than the other cases.. The inability of the simulation to handle the early pilot injection coupled with the late main injection timing is a deficiency. As a result, the NO prediction is not accurate for this particular case. The comparison between experimental and predicted NO values can be found in Table 4. The NO values were predicted using both experimental ROHR and predicted ROHR. This was a means of NO comparison without the error induced through ROHR calculation.

**Table 7- Comparison of predicted and experimental NO (ppm).**

| Engine Case | Exp. NO (ppm) | Pred. NO with exp ROHR (ppm) | Pred. NO with pred ROHR (ppm) | Percent error (pred ROHR) |
|---|---|---|---|---|
| M1 | 161 | 141.3 | 178 | 10.3 |
| M2 | 485 | 921.6 | 1099 | 126.6 |
| M3 | 426 | 335.2 | 523.1 | 22.79 |
| M4 | 114 | 119.4 | 110.6 | 3.106 |
| M5 | 361 | 389.3 | 369.9 | 2.469 |
| M6 | 306 | 295.6 | 314.9 | 2.914 |
| M7 | 88.9 | 110.4 | 101.8 | 14.55 |
| M8 | 276 | 261.8 | 261.8 | 5.159 |
| M9 | 333 | 285.1 | 362.5 | 8.848 |

The target for this simulation was to achieve NO prediction within ten percent. The simulation was carried out using both predicted and experimental ROHR for the NO solution. For most test cases, this was achieved. However, for a few cases this was not accomplished well. Modes 1-3 do not show good prediction as compared to the other 6 modes. As previously stated, M2 is not able to be accurately captured. The injection timings do not lend themselves well to this simulation. If it had been a single injection or

the timing difference between the pilot and main injection were not so vast, the predicted NO would have been accurate. If this mode is omitted, the average error across the other 8 cases is 8.8%. This is acceptable for this simulation. The low load and multiple injection cases are handled well, but the medium and high load cases are typically more accurate across a wider range of applications. This is reinforced with the 6.8L and 9.0L cases, described more completely below. The algorithm predicts especially well for the higher speed cases, but not quite as well for the lower speed cases. This is unexpected because [1] is the primary model for ROHR and the cases examined there were lower speed than those here. Of the medium to higher load cases, the largest relative error occurs with Mode 7. However, this mode is very difficult to return a smaller relative error due to the low experimental NO value. M7 only differs by about 12 ppm, while M9 differs by 30 ppm. M9 returns a smaller relative error however, as the experimental number is so larger. The relative error for the cases using the experimental ROHR is also low at approximately 11.5%. This is slightly higher than the relative error using predicted ROHR, but it is a negligible difference. Using the experimental ROHR helps to validate the NO prediction model, and the fact that they match closely with those determined from the predicted ROHR model is a sign that the ROHR model is close enough to be effective for these cases.

Analysis of just 9 cases is not sufficient to determine if the algorithm works. To further validate the model, an additional 49 cases were used. The agency providing the data wishes for some details to be omitted, but the general operating parameters are noted in the appendix. There were two engines used for this further validation: a 6.8L

and a 9.0L. They are both 6 cylinder engines, and the 6.8L is actually geometrically identical in every way to the currently-studied 4.5L engine besides number of cylinders. At the wishes of the sponsoring agency, the details published here are not as complete as the previous 9 cases, but the algorithms used are identical. Figures 22 and 23 show the NO predicted using the experimental ROHR for both the 6.8L and the 9.0L, respectively.

The operating conditions of the previous 49 cases can be found in the 2.2. The bar graphs in figures 22 and 23 show the experimental NO, predicted NO, and error. There is a very wide range of operating conditions across the spectrum for both engines, but all tuning constants and parameters are unchanged for each case. All cases for the 9.0L engine use substantial EGR, whereas only the first 11 cases use EGR with the 6.8L engine. Cases 12-23 use very little or no EGR at all. These cases are not matched very well in comparison to the cases using significant EGR. However, for the 9.0L most of the cases fall below the 10% error target. For these predictions, the load does not matter because the predictive ROHR is not used. The purpose of figures 22 and 23 is to validate the NO algorithm.

The next step is to look at the same cases using predictive ROHR as in figures 24 and 25. The errors in NO prediction using predictive ROHR are much higher than those of the experimental ROHR. As previously discussed, the low load cases typically pose an issue with accuracy. If these cases are omitted, the average error drops dramatically. Therefore, the authors propose that the algorithm detailed in this work should only be applied to medium and high load cases. The algorithm could likely be tuned using KLA

to be successful for low load cases, but to fit the greatest number of cases it is preferred to utilize the methods with medium and high load cases.

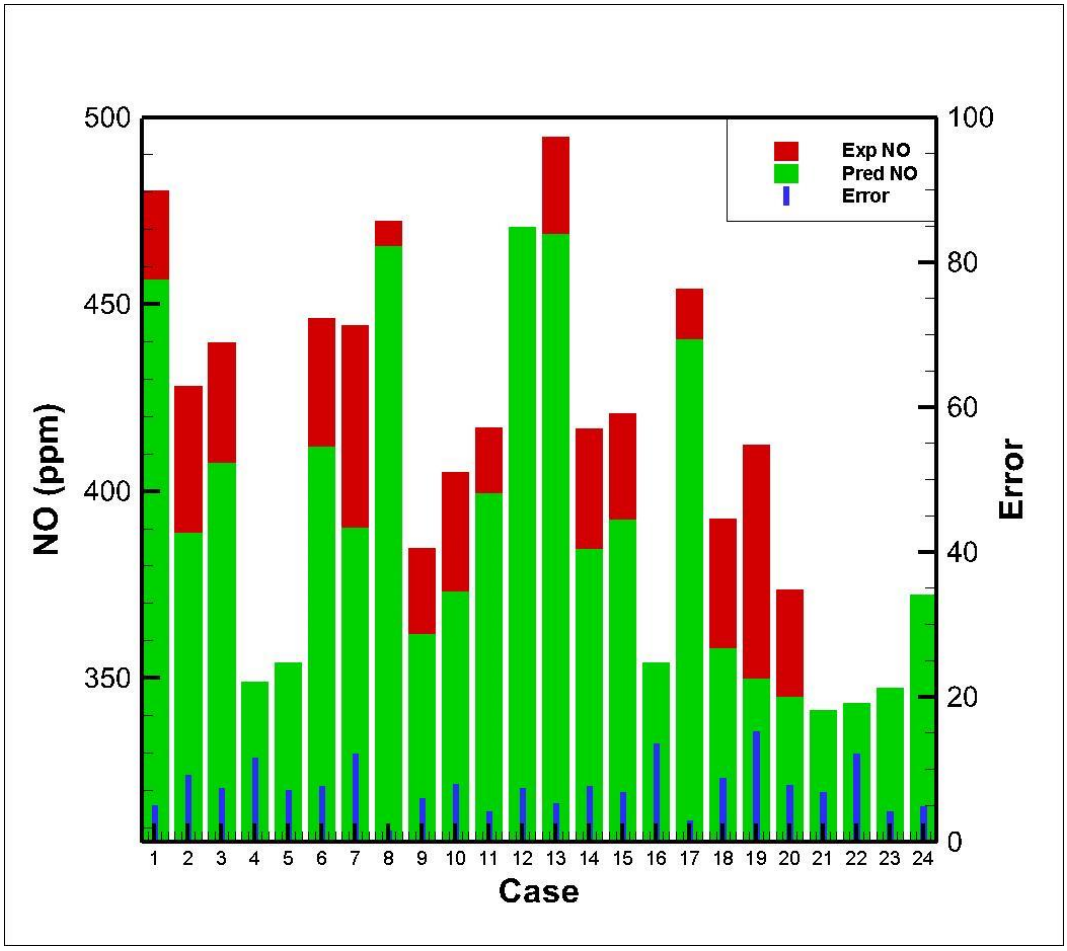


**Figure 22 - NO predicted using experimental ROHR for 9.0L.**

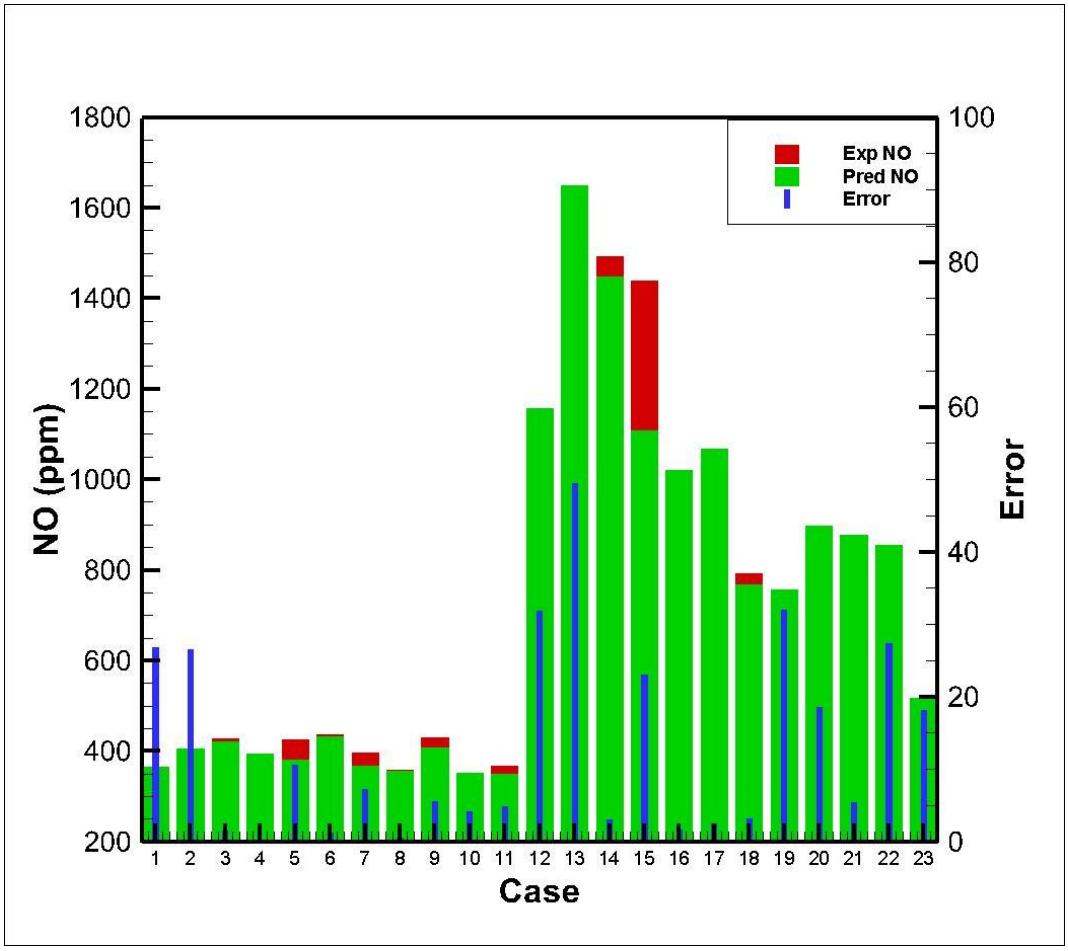


**Figure 23 - NO predicted using experimental ROHR for 6.8L.**

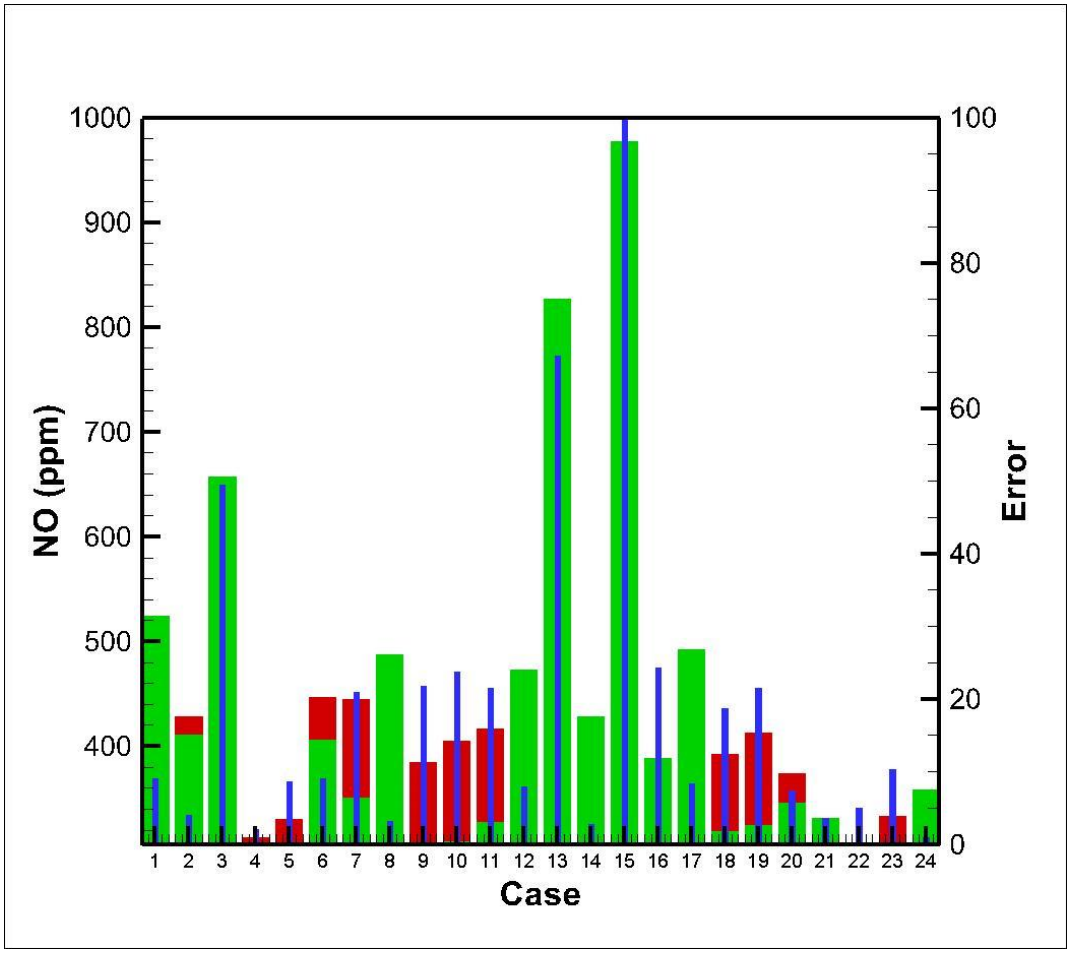


**Figure 24 - NO predicted using predictive ROHR for 9.0L.**

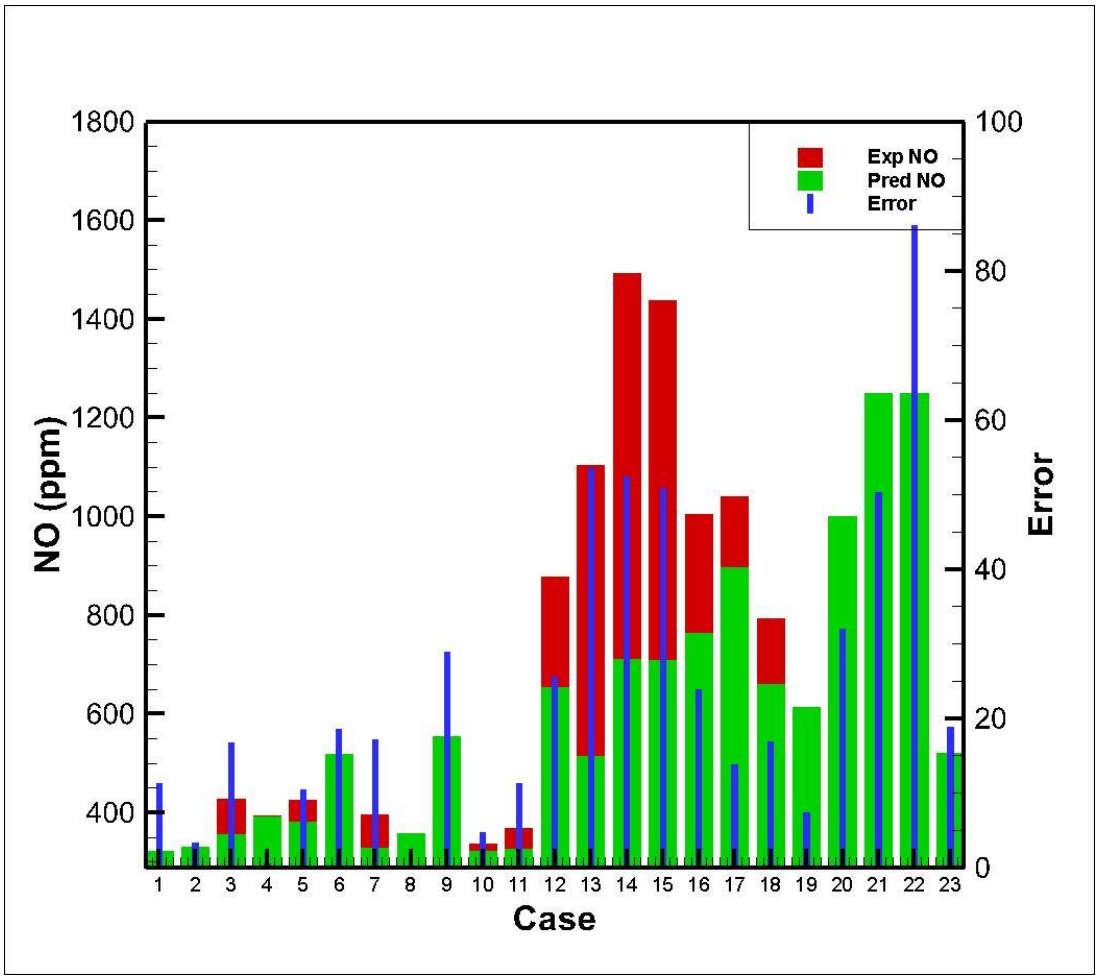


**Figure 25 - NO predicted using predictive ROHR for 6.8**

# 4. NEXT STEPS

To validate the current model, more test cases are required. Multiple injection cases certainly need more exploration beyond the scope of this thesis, but it is likely an algorithm can be designed to accurately model these cases. Comparison with conventional spray models as opposed to that used in [1] and here could be an interesting future work specifically with low load cases.

# 5. CONCLUSIONS

The target of predicting NO within ten percent of the experimental value was attained for the majority of test cases, and the average error was below that with few exceptions. Pressure predictions are not as good as shown in literature, but seem to be reasonable for the purposes of predicting NO. The proposed methodology for predicting temperature appears to be accurate; complete validation, however, will require an even larger experimental data set. The burned zone temperatures agree well with those predicted in [2], building confidence in the temperature prediction model used here. While the predictions are currently within ten percent for most of these cases, more cases should be applied to determine if this algorithm is indeed valid.

The algorithms designed to account for EGR and fuel injection worked well in this application. However, more care must be taken when examining low load data. The spray model used in [1] and recreated here does not predict premixed burning well and focuses more on diffusion burning. While this is acceptable for medium to high load cases, premixed burning is more important in the lower load operating conditions. As a result, the pressure and NO predictions suffer at low load. If low load analysis is desired, it might be beneficial to instead utilize a more traditional spray model with an ignition delay correlation.

Multiple injection cases were also analyzed in this work, and the results seem promising. NO matched acceptably well in all cases except for one. This mismatched

case could probably have been due to errors in the experimental data, but that is difficult to ascertain.

The simulation developed here could be applied with reasonable accuracy without large amounts of tuning. For cases significantly different from those provided here, some minimal changes may be necessary. However, the vast majority of the algorithm presented could be carried over unchanged.

# REFERENCES


1. Eilts, P. and Stoeber-Schmidt, C-P. “Further Development and Application of a Model for the Calculation of Heat Release in Direct Injection Diesel Engines.” SAE Technical Paper. 2014-01-1076, 2014.
2. Welhelmsson, C., Tunestal, P., Johansson, B., Widd, A., Johansson, R. “A Physical Two-Zone NOx Model Intended for Embedded Implementation”. SAE Technical Paper. 2009-01-1509, 2009.
3. Querel, C., Grondin, O., and Letellier, C. “A Semi-Physical NOx Model for Diesel Engine Control.” SAE Technical Paper. 2013-01-0356.
4. Hiroyasu, H. and Kadota, T. “Models for Combustion and Formation of Nitric Oxide and Soot in Direct Injection Diesel Engines.” SAE Technical Paper. 760129, 1976.
5. Heywood, J.B. *Internal Combustion Engine Fundamentals*. “Pollutant Formation an Control.” Pp. 572-577. Print. 1988 McGraw-Hill, Inc.
6. Grahn, M., Johansson, K., Vartia, C., McKelvey, T. “A Structure and Calibration Method for Data-Driven Modeling of NOx and Soot Formation form a Diesel Engine.” SAE Technical Paper. 2012-01-0355.
7. Seykens, X., Willems, F., Kuijpers, B., Rietjens, C. “Automated Model Fit Method for Diesel Engine Control Development.” SAE Technical Paper. 2014-01-1153.
8. Karaky, H., Mauviot, G., Tauzia, X., Maiboom, A. “Development and Validation of a New Zero-Dimensional Semi-Physical NOx Emission Model for a D.I. Diesel Engine Using Simulated Combustion Process.” SAE Technical Paper. 2015-01-1746.

9. Lee, J., Lee, S., Park, W., Min, K., Song, HH, Choi, H., Yu, J., Cho, SH. “The Development of Real-time NOx Estimation Model and its Application.” SAE Technical Paper. 2013-01-0243.
10. Finesso, R. and Spessa, E. “Real-Time Predictive Modeling of Combustion and NOx Formation in Diesel Engines Under Transient Conditions.” SAE Technical Paper. 2012-01-0899.
11. Mellor, A.M., Mello, J.P., Duffy, K.P., Easley, W.L., Faulkner, J.C. “Skeletal Mechanism for NOx Chemistry in Diesel Engines.” SAE Technical Paper. 981450.
12. Sandoval, D. and Heywood, J. “An Improved Friction Model for Spark-Ignition Engines.” SAE Technical Paper. 2003-01-0725.
13. Ghojel, J.I. “Review of the development and applications of the Wiebe function: a tribute to the contribution of Ivan Wiebe to engine research.” International Journal of Engine Research, Vol. 11. JER06510.
14. Walke, N., Marathe, N. and Nandgaonka, M. “Simplified Combustion Pressure and NOx Prediction Model for DI Diesel Engine.” SAE Technical Paper. 2013-26-0131.
15. Solbrig, C. and Litzinger, T. “The Effect of Intake Charge Temperature on Combustion and Emissions in an Optically Accessible DI Diesel Engine with and without Swirl.” SAE Technical Paper. 902060.
16. Lakhlani, H., Barman, J., Rajput, K., and Goswami, A. “Experimental Study of EGR Mixture Design and its Influence on EGR Distribution Across the Cylinder for NOx-PM Tradeoff.” SAE Technical Paper. 2013-01-2743.

17. Gatowski, J.A., Balles, E.N., Chun, K.M., Nelson, F.E., Ekchian, J.A., and Heywood, J.B. “Heat Release Analysis of Engine Pressure Data.” SAE Technical Paper. 841359.